Engineering Failure Analysis 118 (2020) 104804

Contents lists available at ScienceDirect

Engineering Failure Analysis

journal homepage: www.elsevier.com/locate/engfailanal

Influence analysis of the geometrical parameters on the electro-mechanical stability of HTS Roebel cables

S. Gijoy, K.E. Reby Roy*

Department of Mechanical Engineering, TKM College of Engineering, Kollam, Kerala, India

ARTICLE INFO

Keywords:
AC loss
Electro-mechanical
Geometry
HTS
Roebel cable

ABSTRACT

Under high-power applications, high-temperature superconducting (HTS) Roebel cables may subjected to heavy tensile load due to electromagnetic forces or due to external factors during the production process of these cables. The meander structure of Roebel strands is prone to these loads which mechanically weakens the stability of Roebel cables due to localized stress concentration. The applied transport current and exposure to an external or self-magnetic field induce AC loss in Roebel cables. In the present work, the influence of geometrical parameters on the electro-mechanical stability of Roebel cables is carefully investigated using 3D finite element tools. The parameters such as inner fillet radius, outer fillet radius, Roebel angle, strand width at crossing section and the gap between stacks of strand in the straight section are varied and its influence on mechanical stability and electromagnetic characteristics are observed. First a default geometry is modelled and its electro-mechanical simulation is performed against various load conditions. Each parameters of the Roebel cable are then altered on this default geometry. After each set of variation, electro-mechanical simulations are performed and its influence is compared with the default geometry.

1. Introduction

Alternating current (AC) of high density, especially in the kA/mm^2 range without much loses are generated easily after the discovery of High-Temperature Superconductors (HTS) [1]. Since then, HTS has become a solution for high-power machines such as superconducting magnets, accelerators and similar electrical devices. HTS is integrated into certain cable structures as thin layer which include Roebel cable [2], conductor on round core (CORC) cable [3] and twisted stacked-tape cable [4] as the current transferred through a single HTS strand cannot meet the power requirement of these high-energy devices. The meander shaped Roebel cable retain a transposed structure which minimizes the current imbalance among strands, reduce AC losses and provides high current carrying potential [5-7].

Under high-power applications, conductors may subjected to heavy tensile load due to electromagnetic forces or due to external factors during the production process of these cables. The meander structure of Roebel strands is prone to these loads which mechanically weakens the stability of Roebel cables due to localized stress concentration. The geometrical parameters of the Roebel cable plays a crucial role in reducing its rigidity and stability [8]. In a multi-stranded cable carrying high transport current, the strands are not only subjected to its self-field, but also to the fields generated by other strands. Also the position of each strand in the cable plays a vital role in the current carrying capability of the entire cable [9]. Hence, the AC loss of Roebel cables due to transport current and magnetization needs to be carefully observed and studied, as the meander shape and transposition of each strand in the

* Corresponding author.
E-mail address: rebyroy@tkmce.ac.in (K.E. Reby Roy).

https://doi.org/10.1016/j.engfailanal.2020.104804
Received 2 May 2020; Received in revised form 29 July 2020; Accepted 4 August 2020
Available online 06 August 2020
1350-6307/

Roebel cable shifts the position of each strand along its length.

In the present work, the influence of geometrical parameters on the electro-mechanical stability of Roebel cables is carefully investigated. The parameters such as inner fillet radius, outer fillet radius, Roebel angle, strand width at crossing section and the gap between stacks of strand in the straight section are varied and its influence on mechanical stability and electromagnetic characteristics are observed. Limited authors studied the influence of geometrical variation in the electro-mechanical performance of Roebel cable. The variation in transport AC losses of Roebel cables with different strand number and width was investigated by [10]. They developed and successfully validated a technique to scale AC losses in Roebel cables with different characteristics which include width, inter strand gap and number of strands. In the study conducted by [8], they overlooked the sub-layers in each Roebel strand and considered it as a monolithic strand made of single material with thickness 0.1 mm and mechanical properties equal to the weighted average ratio of stabilizing layers and the substrate. And the electromagnetic analysis was performed using 2D FEM simulation. The variation of AC losses in Roebel cables with variation in geometrical parameters such as the number of strands, the transposition length, and the width of the gap between stacks of strand in the straight section was studied in the work [11]. Here the thin strip approximation method was used and the superconducting layers were treated as surfaces. However, in the present work the authors tried to simulate both 3D mechanical and electromagnetic analysis of a Roebel strand/cable whose specification is very close to the real case 2G HTS Roebel strand/cable. In the present work all studies/simulations are conducted at 77 K. Since the relevance of HTS cables in potential applications is inevitable, the real-world physical conditions of HTS cables need to be simulated using 3D finite element tools that help to design and develop advanced cables.

2. Mechanical investigation

The influence of varying various geometrical parameters of the Roebel strand in their mechanical stability is analyzed using finite element method. The meander shaped Roebel strands are modeled using SOLIDWORKS 2014 and its simulation is performed using Ansys 19.1. The 3D models of the Roebel strand are assumed to be punched off from the 2G HTS SCS4050 tape. First a default geometry is modelled and its mechanical stability against an externally applied tensile load is simulated. Then each geometrical parameters of the Roebel strand are varied on this default geometry. After each set of variation, tensile load simulations are performed and its influence is compared with the default geometry. Tensile load is given to one end face of the model as displacement constraint and its influence on mechanical stability is evaluated by plotting stress-strain graphs.

2.1. Model description for mechanical analyses

The Roebel strand for analysis is assumed to be punched off from the 2G HTS SCS4050 tape manufactured by SuperPower [12]. The 3D structure of such a tape modelled in SOLIDWORKS 2014 is shown in Fig. 1.

For studying the influence of variation of geometrical parameters on the mechanical stability of Roebel cable, a default geometry is first considered. The specification of the default geometry of the Roebel strand is mentioned in Table 1. The default geometry in this paper means the reference geometry from which the variations are made on each parameter to evaluate their influence in transmitting tensile load. A single strand of specification mentioned in Table 1 is shown in Fig. 2. The 2D representation of a small portion of the Roebel cable is exhibited in Fig. 3.

The structure of a Roebel cable consists of parts such as cross-over section (W_x), straight section (W_R), outer corner, inner corner, Roebel angle (φ), inner radius, outer radius, transposition length ($2L$), gap between stacks of strand at the straight section (W_c) etc. [2,8]. If the connection between straight portion and the cross-over region of a Roebel strand is sharp, it is considered as an inner corner/outer corner. Providing a fillet makes this region smooth, then it is called inner radius/outer radius. The choice of inner or outer region relies on the alignment of the strand. The regions are clearly indicated in Fig. 3 and Fig. 4.

In the present work, the model considered for finite element (FE) mechanical simulation ignored both the silver over-layers and the buffer layers because their influence on mechanical stability of the cable is too small [13]. The geometry considered for the simulation is given in Fig. 5.

The authors also simulated the steps involved in the production process of Roebel strand to find out the remanent strain in the superconducting layer which greatly influence the critical strain of the Roebel strand under tensile load. The steps adopted for

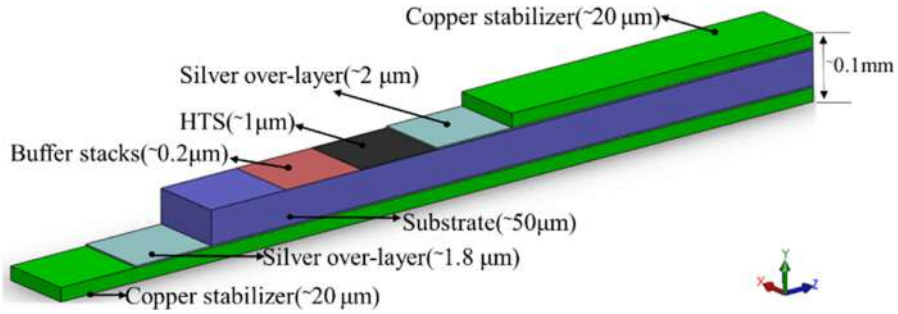

Fig. 1. 3D representation of 2G HTS SCS4050 tape (modelled in SOLIDWORKS 2014).

Table 1
Specifications of the default Roebel strand punched off from the SCS4050 tape.

Parameters	Values
Width of the tape (W_t)	4 mm
Strand width of straight section (W_R)	2 mm
Strand width at transposition section (W_x)	2 mm
Thickness of Hastelloy substrate	50 μm
Thickness of superconducting layer(approx.)	1 μm
Thickness of Copper stabilisation layer (on each side)	20 μm
Gap between stacks of strands in the straight section (W_c)	Nil
Transposition length (cabling pitch) (L)	109 mm
Roebel angle (φ)	30°
Total thickness of Roebel strand (approx.)	0.1 mm

Fig. 2. Two different orientations of a Roebel strand detached from a Roebel cable. (a) Top view of a Roebel strand (b) Side view of a Roebel strand.

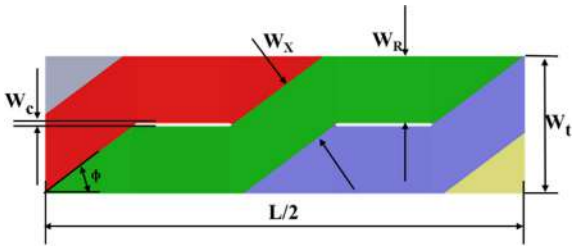

Fig. 3. The 2D structure of a Roebel cable (modelled in SOLIDWORKS 2014).

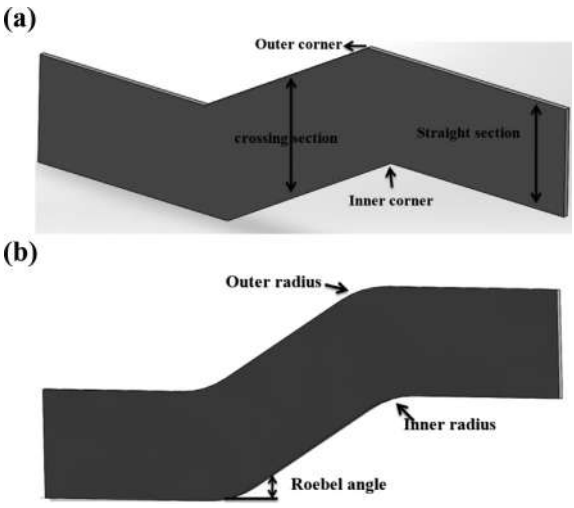

Fig. 4. The cross-over region of Roebel strand. (a) Strand with sharp inner and outer corners. (b) Strand with radial fillet provided.

simulation is represented in Fig. 6.

The following series of steps is considered for the simulation of Roebel strand: first, the ReBCO film is coated on the substrate using the metal–organic chemical vapour deposition (MOCVD) at 1020 K. The electroplating of copper is performed after cooling the system to 350 K [14]. After cooling the HTS tape to room temperature (RT), Roebel strand is punched out from the strand using

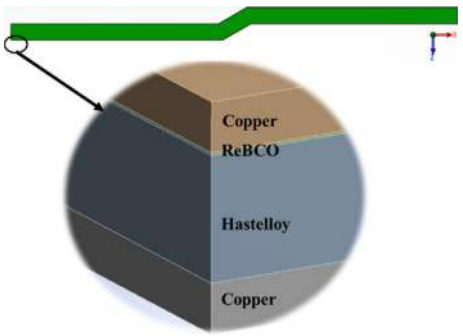

Fig. 5. Periodic region in a Roebel strand taken for simulation. Enlarged view at one end of the strand is also given to show the sub-layers considered in the model.

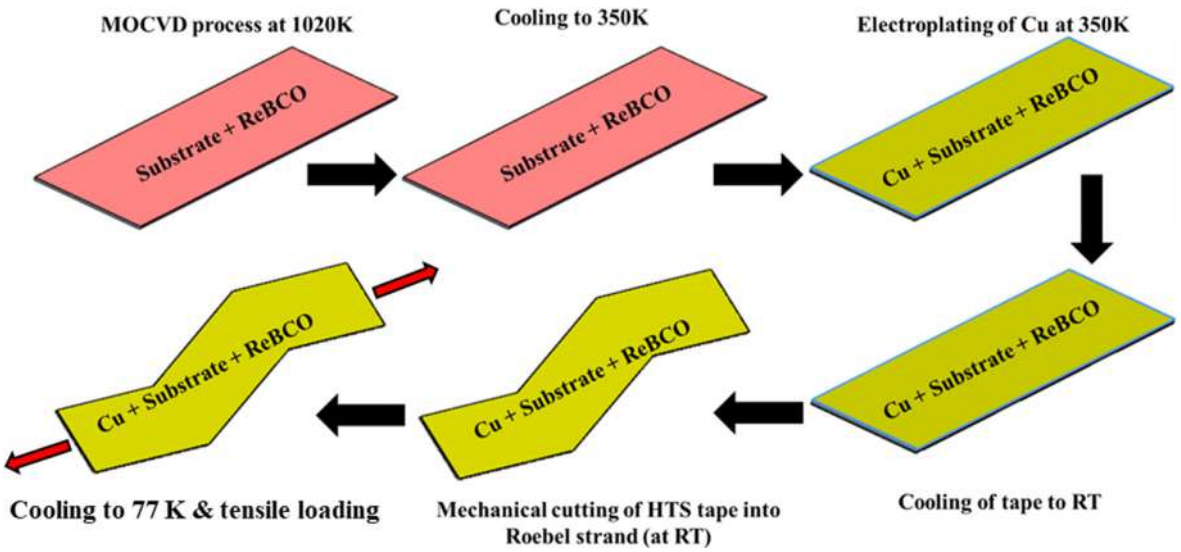

Fig. 6. Steps involved in the finite element simulation of the HTS Roebel strand.

mechanical punching method [2]. Tensile test simulation is then carried out once the strand is cooled to 77 K.

2.2. Material properties and boundary conditions

The configuration of an SCS4050 HTS tape includes copper stabilizer layers, silver over-layers, buffer layers, ReBCO (Rare-earth barium copper oxide) superconducting layer and the Hastelloy substrate [12]. However, the present work ignored the silver over-layers and the buffer layers as mentioned earlier. It is assumed that the tape materials are isotropic. The properties of the materials considered for analysis are mentioned in Table 2.

The elasto-plastic behavior of SCS4050 tape, Hastelloy and copper at 77 K and room temperature were taken from the tensile stress-strain loading experiments presented in [14]. The characteristics of Hastelloy and copper in its plastic range obtained from [14] are provided as digitized figures into the nonlinear sections of the stress-strain curves in the finite element model. The elasto-plastic properties of both Hastelloy and copper beyond room temperature are considered equivalent to that at room temperature and the thermal expansion coefficient is assumed consistent at any temperature. The variation of material properties with temperature is

Table 2
Material properties of Hastelloy and copper at RT and 77 K [14]

Material	Young's modulus (Gpa)	Yield stress (MPa)	Poisson ratio	Thermal expansion coefficient (K-1)
Hastelloy (at RT)	223	891	0.307	1.34E-05
Hastelloy (at 77 K)	228	1141	0.307	1.34E-05
Copper (at RT)	80	120	0.34	1.77E-05
Copper (at 77 K)	98	146	0.34	1.77E-05
ReBCO	157		0.3	1.10E-05

considered linear between 77 K and room temperature.

Due to the periodic repetition of the cross-over region of a Roebel strand, the model taken for simulation considers only half of its transposition length. A similar assumption and modelling procedure can be seen in [15]. One end face of the model (represented in Fig. 5) is given symmetry boundary condition and to the other end face tensile load is given as displacement constraint (along x-axes) by 1% strand deformation. Grid independent analysis was performed, and the adequate range of elements and dimensions were determined to confirm that sufficient FE mesh resolutions were used. Each layer of the strand has discretized with 3D hexahedral elements.

In the present work, the axial strain at which the crack begins in the ReBCO layer is taken as the reference to evaluate the influence of variation in strand parameters on the performance of the strand under tensile load.

2.3. Simulation method

The default geometry considered for the simulation is shown in Fig. 5. In a Roebel strand, each sub-layer has its own specific function. But the potential of HTS Roebel strand depends on the performance of the ReBCO layer against externally applied loads. A Roebel strand subjected to an external load enough to create a crack in the ReBCO layer, can result in the critical current degradation of the whole strand, thereby affecting the cable performance. When an SCS4050 tape is subjected to a tensile strain (in the longitudinal direction of the tape's orientation) of 0.7% at 77 K, the formation of crack get initiated in the superconducting film at an intrinsic axial strain of 0.45% [13]. In another work [14], the validation of 0.45% criterion is performed by comparing the experimental and simulated result of an SCS4050 tape subjected to external tensile load. The work also suggested that the proposed model (the 0.45% criterion) can be effectively used to determine (optimize) the critical stress/strain of cable models such as CORC, twisted stack-tape or Roebel cable.

In the present work, the 0.45% criterion is used to determine the axial strain at which the crack initiates in the ReBCO layer and the corresponding applied strain and stress on the strand is considered as the critical stress and strain of the Roebel strand. The critical stress/strain is the stress/strain at which the critical current is going to degrade in a HTS Roebel strand. The peak value of applied strain and critical stress at which the crack initiates in the ReBCO layer of an associated geometrical configuration can be considered as an indication of the response of Roebel strand to tensile loads. High value of critical stress against an applied strain means, the geometrical configuration under consideration can withstand more load without any distortion or critical current degradation. Likewise, low values of critical stress and applied strain means the crack has initiated in the ReBCO layer at an early strain and such a Roebel cable may fail to conduct critical current at large applied loads.

First, the simulation is performed on the default geometry Roebel configuration and its critical stress and corresponding applied strain are observed. Simulations are then performed on all other Roebel cable configurations with different set of geometrical parameters, while maintaining the same boundary conditions. The dependence of various geometrical parameters on the mechanical stability of Roebel strand is then investigated in comparison with the default geometry. The relative values are taken into consideration to simplify the comparison with the default geometrical configuration. For example, relative critical stress/strain is the ratio of critical stress/strain obtained from the simulation of geometrical configuration under consideration to the default geometrical configuration of the Roebel strand. The specification mentioned in Table 1 is preferred as the default geometrical configuration, since several authors investigated the performance of the Roebel cable using these specific sets of geometric parameters [2,8,16,17]. However, a transposition length of 109 mm is considered to reduce the computational effort.

The surface plot of the distribution of strain in the ReBCO layer at 77 K of the Roebel strand punched off from the SCS4050 tape is given in Fig. 7. It is noticed that the stress is concentrated at the sharp inner corners of the ReBCO layer. The axial strain at which the crack is initiated in the ReBCO layer and its corresponding stress on the Roebel strand is taken for analysis. It is to be noted that crack is initiated in the ReBCO layer when the axial strain in it reaches 0.45% [14]. The study conducted by [7] conveyed that the Roebel strand collapses (degradation of critical current begins) soon compared to the SCS4050 HTS tape because of the bizarre failure mechanism occurs in it during tensile loading. At the cross-over region of the Roebel strand, it undergoes an out-of-plane twisting under tension and stress re-distributes within the strand. However, the stress get localized at the inner corner of Roebel strand and the resulting strain in the ReBCO layer at this area becomes 0.45%.

2.4. Governing equations

The static structural module in the software tool Ansys 19.1 solve the domain under consideration using the governing equations such as equilibrium equations, strain-displacement relations and stress-strain relations. The equations are given by:

$$\frac{\partial \sigma_x}{\partial x} + \frac{\partial \tau_{xy}}{\partial y} + \frac{\partial \tau_{xz}}{\partial z} + f_x = 0 \tag{1}$$

$$\frac{\partial \tau_{xy}}{\partial x} + \frac{\partial \sigma_y}{\partial y} + \frac{\partial \tau_{yz}}{\partial z} + f_y = 0 \tag{2}$$

$$\frac{\partial \tau_{xz}}{\partial x} + \frac{\partial \tau_{yz}}{\partial z} + \frac{\partial \sigma_z}{\partial y} + f_z = 0 \tag{3}$$

Where σ_x, σ_y, σ_z are the normal stresses, τ_{xy}, τ_{xz}, τ_{yz} are shear stresses and f_x, f_y, f_z are the components of forces.

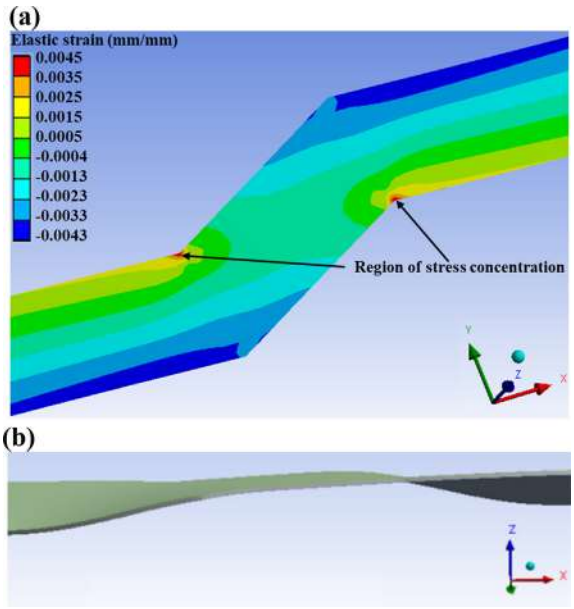

Fig. 7. (a) Dispersal of strain in the superconducting layer of a deformed Roebel strand. Colour scale indicates the intensity and distribution of strain in the strand. (b) Deformed Roebel strand showing its out-of-plane twisting under applied tensile load.

$$\epsilon_x = \frac{\partial u_x}{\partial x} \tag{4}$$

$$\epsilon_y = \frac{\partial u_y}{\partial y} \tag{5}$$

$$\epsilon_z = \frac{\partial u_z}{\partial x} \tag{6}$$

$$\gamma_{xy} = \frac{\partial u_x}{\partial y} + \frac{\partial u_y}{\partial x} \tag{7}$$

$$\gamma_{yz} = \frac{\partial u_y}{\partial z} + \frac{\partial u_y}{\partial y} \tag{8}$$

$$\gamma_{zx} = \frac{\partial u_z}{\partial x} + \frac{\partial u_x}{\partial z} \tag{9}$$

Where u_x, u_y, u_z are unit displacement, ϵ_x, ϵ_y, ϵ_z are normal strains and γ_{xy}, γ_{yz}, γ_{zx} are the engineering shear strains.

$$\epsilon_x = \frac{\sigma_x}{E} - \nu\frac{\sigma_y}{E} - \nu\frac{\sigma_z}{E} + \alpha\Delta T \tag{10}$$

$$\epsilon_y = \frac{\sigma_y}{E} - \nu\frac{\sigma_z}{E} - \nu\frac{\sigma_x}{E} + \alpha\Delta T \tag{11}$$

$$\epsilon_z = \frac{\sigma_z}{E} - \nu\frac{\sigma_x}{E} - \nu\frac{\sigma_y}{E} + \alpha\Delta T \tag{12}$$

$$\gamma_{xy} = \frac{\tau_{xy}}{G} \tag{13}$$

$$\gamma_{yz} = \frac{\tau_{yz}}{G} \tag{14}$$

$$\gamma_{zx} = \frac{\tau_{zx}}{G} \tag{15}$$

where E, G, ν, α and ΔT are the Young's modulus, modulus of rigidity, Poisson's ratio, coefficient of thermal expansion and change in temperature respectively.

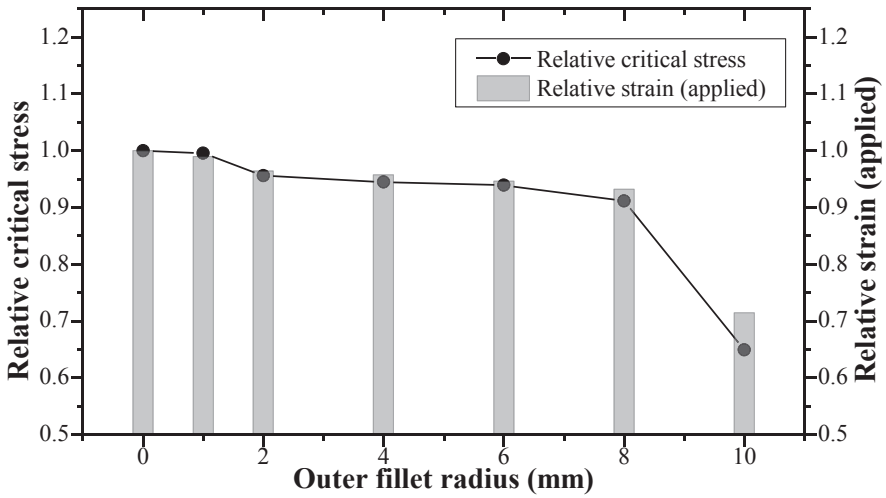

Fig. 8. Graph showing the performance of Roebel strand under various outer fillet dimensions.

2.5. Result and discussions

The influence of providing fillet at the outer corner of a Roebel strand is represented in Fig. 8. The simulated result shows that providing fillet on the outer corner of a Roebel strand reduces its mechanical stability. From the figure one can infer that increasing the dimension of fillet at the outer corner increase the sensitivity of the Roebel strand against externally applied tensile load and the degradation of current may occur at an earlier applied strain. So it is better to leave the outer corner of the Roebel strand always sharp as recommended in [8].

It can be noticed that providing fillet at the outer corner of the Roebel strand causes removal of material from the default geometrical design, which increases as the fillet size increases. This reduces the strength of the strand, which is visible from its performance against externally applied loads. The reduction of critical stress/strain up to 8 mm is gradual and after that the variation is rapid. This is due to the fact that further increase in size of outer fillet takeaway the meander shape of the Roebel strand and in addition to that the width of the strand at the beginning of the cross-over region decreases due to material removal.

Fig. 9 shows the distribution profile of axial strain in the ReBCO layer of a Roebel strand of outer fillet dimension equals 4 mm. Similar plots were observed from the simulated result of all Roebel configurations with different outer fillet dimensions; the only variation is obtained in the magnitude of the applied strain and the corresponding critical stress.

Fig. 10 shows the dependence of inner radii against externally applied tensile load. From the figure, it can be inferred that increasing the inner fillet radius increases the strength of the Roebel strand. Providing inner fillet distributes the stress over a larger area, rather than concentrating it at the sharp inner corner as visible in the surface plot presented in Fig. 11. The redistribution of stress enhance the performance and enables the Roebel strand to conduct critical current without any degradation under more tensile load compared to the strand with sharp inner corners [8]. However, too much increase in inner fillet dimension is not possible as it may take away the meander structure of the Roebel strand. Also, further increase in inner fillet dimension can only be achieved by

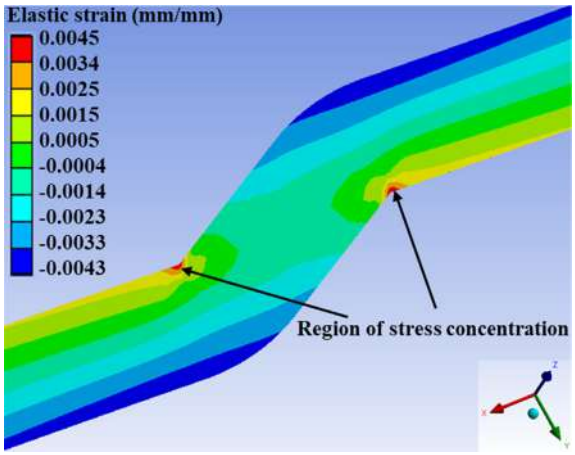

Fig. 9. Surface plot of the dispersion of strain in the superconducting layer of a Roebel strand with 4 mm outer fillet after crack initiation.

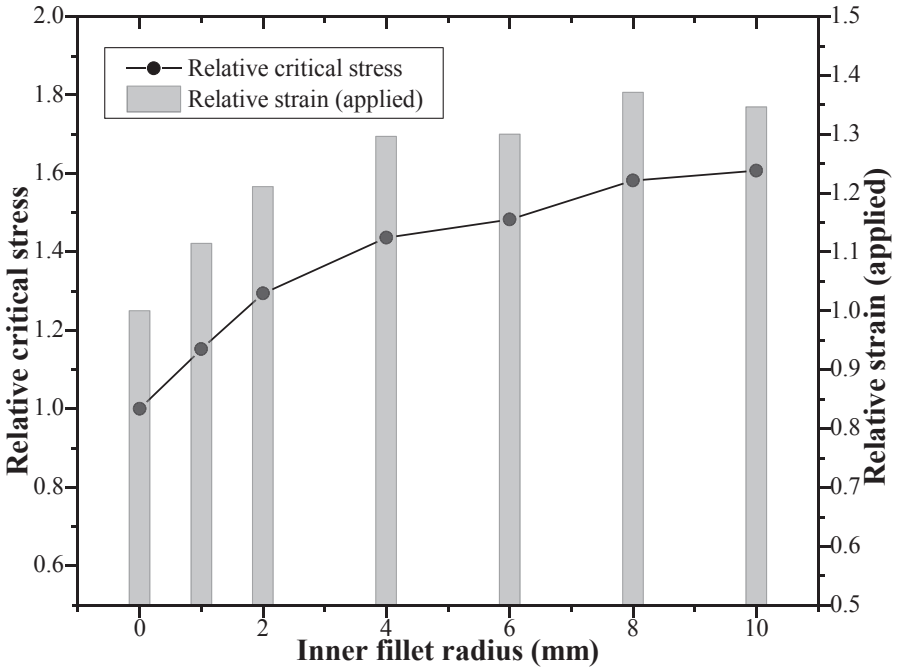

Fig. 10. Graph showing the influence of varying inner fillet size on the critical stress and applied strain of a Roebel strand.

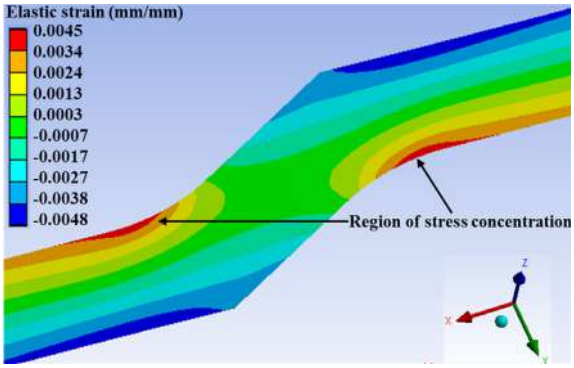

Fig. 11. Simulated result of distribution of axial strain in the ReBCO layer of a Roebel strand with inner fillet 4 mm.

restricting the number of strands in the Roebel cable; which means the number of strands in a cable with a fixed transposition length will get reduced if we increase the dimension of inner fillet. For example, the maximum possible fillet dimension for a 14-strand Roebel cable with specification mentioned in Table 1 is 6 mm.

The dispersion of axial strain in the superconducting layer for all inner fillet size confirms that as the inner fillet dimension increases, the stress distributes over a wider area and magnitude of critical stress and corresponding applied strain varies.

Selection of the appropriate Roebel angle plays an important role in the mechanical stability of Roebel cable against external applied loads. The effect of varying Roebel angle and its dependence on applied strain and corresponding stress of a Roebel strand is investigated and shown in Fig. 12. The number of strands in a Roebel cable with a given transposition length also depends on the selected Roebel angle. If the angle is less, then the number of strands that can be occupied in a cable of given transposition length is less, and vice versa. However, the increase in Roebel angle limits the size of inner fillet that can be provided on a cable with maximum number of strands. For example, the Roebel angle that can be provided on a Roebel cable (of specification mentioned in Table 1) with strand of 6 mm inner fillet is between 15° and 45°. Even though the increase in Roebel angle reduces the possibility of crack initiation in the ReBCO layer at an early strain, the length of cross-over region get reduced and it will affect the true meander structure of Roebel strand. Due to the specific meander shape of the Roebel strand, there occurs an out-of-plane twisting when a tensile load acts on it [7]. Out-of-plane twisting of the Roebel strand against a tensile load is greatly influenced by the Roebel angle. It is noticed that at each Roebel angle selected for simulation, the degree of twisting in the Roebel strand due to tensile loading is different, which is the main cause of increased critical stress at some angles.

The distribution of axial strain in the ReBCO layer of the HTS Roebel strand at various Roebel angle shows similar surface plot.

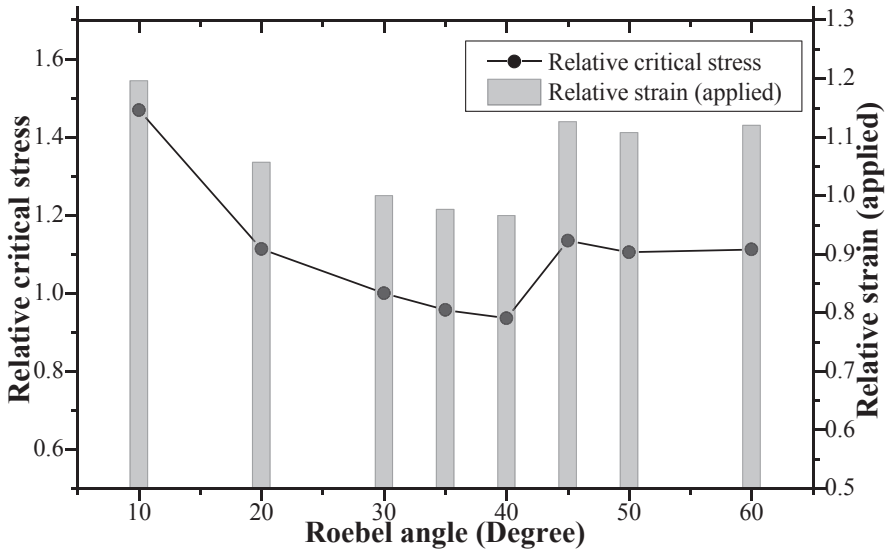

Fig. 12. Graph showing the dependence of Roebel angle on the mechanical stability of a Roebel strand.

However, difference is noted in the magnitude of the critical stress and corresponding applied strain.

From Fig. 13, it can be observed that as the relative width of the Roebel strand increases the mechanical strength increases and the corresponding strain at which the crack initiates in the ReBCO layer also increases. The relative width of a Roebel strand is the ratio of the width of the strand at cross-over region (W_x) to the width of the strand at straight section (W_R).

When the relative width increases, the area of load distribution in the cross-over region of the Roebel strand increases, thereby increasing the mechanical stability of the strand against external load. Although wide variation is observed in the strength of the strand, much increase is not experienced in the stability of ReBCO strand against applied tensile load. Since the increase in relative width greatly influence the space requirement of each strand in the Roebel cable which further reduces the number of strands in a given configuration, a relative width between 1 and 1.2 is recommended for Roebel structures [8].

The simulated distribution profile of axial strain in the ReBCO layer of the Roebel strand at different relative width looks similar and variation is observed in the magnitude of the critical stress and corresponding applied strain. It is also noticed that the stress distribution in the cross-over region increases as the relative width increases.

The impact of varying gap between stacks of strand at the straight section of the Roebel cable on the mechanical stability of

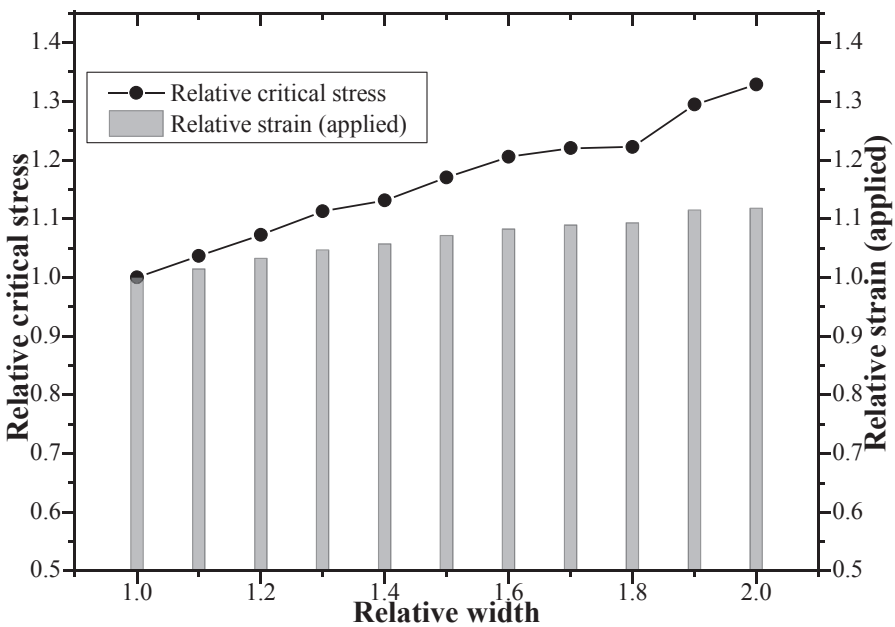

Fig. 13. Graph representing the effect of variation in relative width on the mechanical stability of a Roebel strand.

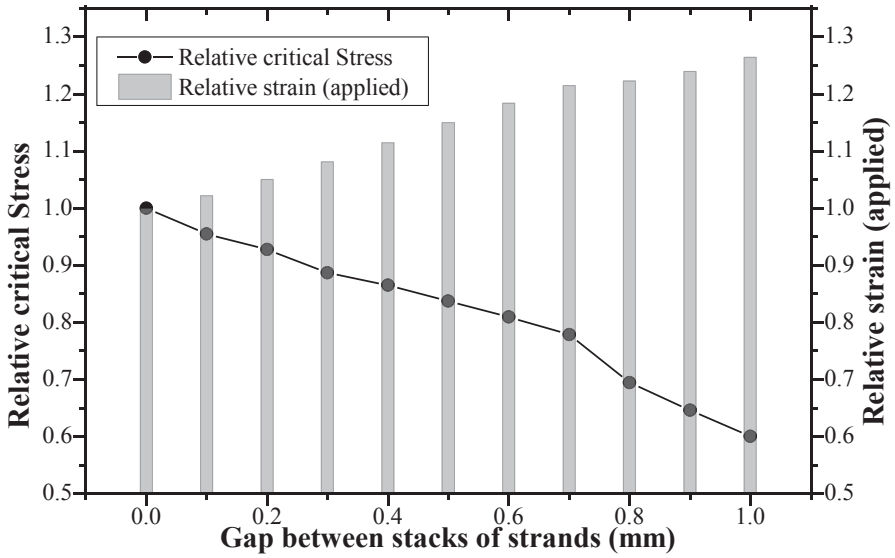

Fig. 14. Graph showing the dependence of gap between stacks of strands at the straight section of Roebel strand on mechanical stability.

Roebel strand is simulated using finite element method and the observed result is represented in Fig. 14. One can notice that when the inter strand gap increases, the critical stress reduces and the corresponding strain applied on the strand increases. As the gap between stacks of strand increases, due to the specific meander structure of the Roebel strand, the degree of out-of-plane twisting of the strand increases with increase in applied tensile load. Most of the applied tensile load causes an uneven twist instead of being distributed into the strand. Hence the resulting axial strain in the ReBCO layer reduces and the strand fails (degradation of critical current begins/the crack initiates in the ReBCO layer) at a lower strain even though applied strain on the Roebel strand is high.

It should be noted that the authors considered to increase the width of the HTS tape to obtain the required gap between stacks of strands in the straight section to maintain the other geometrical parameters of the Roebel strand mentioned in Table 1.

3. Electromagnetic investigation

The 3D electromagnetic analysis and simulation of a Roebel cable with varying geometrical configuration is investigated using finite element method. The FE tool Ansys 19.1 is used for the simulation. The performance of the Roebel cable with varying geometrical parameters are studied in two test cases i) an alternating magnetic field in perpendicular direction is applied to the widest face of the Roebel cable ii) an alternating transport current is applied to the Roebel cable.

3.1. Model description for electromagnetic analyses

For the analysis a 14-strand Roebel cable is considered and its specification is mentioned in Table 3. The 3D structure of a Roebel cable with 14 strands is represented in Fig. 15. The 3D meander structure of Roebel cables possess a recurring section created due to the transposition of one strand over the other. Hence the computer effort can be minimized by considering such a repetitive zone shown in Fig. 16 for simulation.

Table 3
Specifications of the default Roebel cable.

Parameters	Values
Width of the tape (W_t)	4.1 mm
Strand width of straight section (W_R)	2 mm
Strand width at transposition section (W_x)	2 mm
Thickness of Hastelloy substrate	50 μm
Thickness of superconducting layer(approx.)	1 μm
Thickness of Copper stabilisation layer (on each side)	20 μm
Thickness of silver over-layer (on each side)	2 μm
Gap between stacks of strands in the straight section (W_c)	0.1 mm
Transposition length (cabling pitch) (L)	109 mm
Roebel angle (φ)	30°
Total thickness of Roebel strand (approx.)	0.1 mm
Number of strands	14

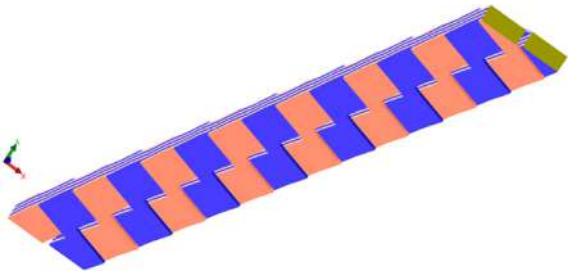

Fig. 15. 3D structure of a 14-strand Roebel cable modelled using SOLIDWORKS 2014.

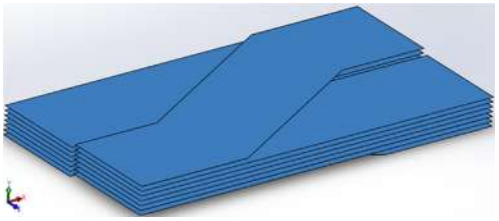

Fig. 16. 3D model of the Roebel cable geometry considered for electromagnetic simulation. Only the repetitive transposition section is represented.

3.2. Governing equations

The electromagnetic simulation uses the governing equations available within the electromagnetic module of the software tool Ansys 19.1 which include the Maxwell equations. The important equations include:

$$\nabla x H = J + \frac{\partial D}{\partial t} \tag{16}$$

$$\nabla x E = -\frac{\partial B}{\partial t} \tag{17}$$

$$\nabla . B = 0 \tag{18}$$

$$\nabla . D = \rho \tag{19}$$

$$J = \sigma E \tag{20}$$

where H is the magnetic field intensity, J is the current density, D is the electric flux density, t is the time, E is the electric field intensity, B is the magnetic flux density, ρ is the electric charge density and σ is the electrical conductivity.

The loss is estimated by the volume integration of the loss per unit volume,

$$P = \int_V P_v(B) dV = \sum_{i=1}^{N} P_v(B_i) \Delta V_i \tag{21}$$

and

$$P_v \alpha B_{max}^2 \tag{22}$$

where N is the total number of mesh elements of the domain, B_i is the flux density at the center of the i^{th} element, ΔV_i is the volume of the i^{th} element, B_{max} is the maximum flux density and f is the applied frequency.

3.3. Material properties and boundary conditions

ReBCO layer in the strand, due to its high conductivity transmits all the current through it when an alternating current is supplied to the Roebel cable [18]. Hence, the present work, in its 3D model, considers only the superconducting ReBCO layer and the air surrounding the Roebel cable for electromagnetic simulation. All geometric configurations (model) presented in the transport current session of this paper are supplied with an alternating current varying from $0.1I_c$ to I_c, where I_c is the critical current of 14-strand Roebel cable which is taken as 465 A [18]. Hence the critical current density is considered as 1.66E10 A/m^2. The frequency of the transport current is fixed at 50 Hz and the impact of displacement current and eddy effects are ignored. For the models presented in the magnetization session, an alternating magnetic field varying from 0.01T to 0.1T at 50 Hz is applied in perpendicular direction to the broad face of the Roebel cable.

$YBa_2Cu_3O_{7-\delta}$ is taken as the ReBCO material and the electro-mechanical properties corresponding to 77 K are considered for the analysis. The work done by [19] describes further details regarding the material properties and boundary conditions in which the 3D

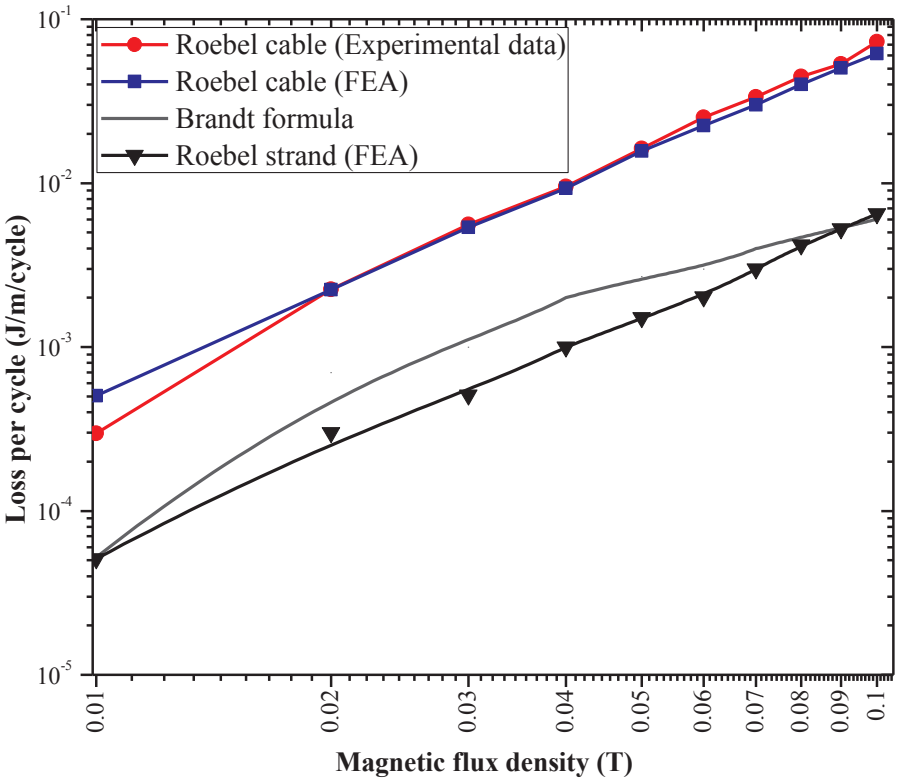

Fig. 17. Magnetization AC losses in Roebel strand and cable. FEA data were obtained from the simulation. Data points labelled Brandt formula were calculated using Brandt-Indenbom equation [23] for a single strand. Experimental data were taken from [18].

finite element electromagnetic analysis of a 14-strand HTS Roebel cable was performed using finite element method and the results are successfully compared and validated with the numerical and experimental result presented in [18] and [20] respectively.

Various types of losses associated with each sub-layer of the HTS tape is presented in the work [21] and it is reported that the major portion of losses incurred in superconducting material is only hysteresis loss. Since the proposed model in the present work takes into account only the superconducting ReBCO layer, the AC loss in the Roebel cable is estimated by calculating the Hysteresis loss. The hysteresis loss in a Roebel cable is very much higher and crucial than the coupling loss, if an alternating magnetic field is introduced in the cable in perpendicular direction to its widest surface [22]. Hence, the current work perceives only the hysteresis loss while evaluating the total AC loss in a Roebel cable under applied alternating magnetic field. Mesh convergence and optimization studies were performed, and the appropriate quantity and quality of elements and its size has been determined to confirm that adequate FE mesh resolutions were used in the model for simulation. Each layer of the strand has discretized with 3D tetrahedral elements.

The magnetization and transport current losses per cycle per unit length of a Roebel strand and cable are shown in the Figs. 17 and 18 respectively. These figures present a comparison between the FEA and experimental result of a 14-strand Roebel cable at different load conditions. The figures also show the deviation of the FEA result from the Brandt formula and Norris formula (strip) applied to a Roebel strand at different magnetic field and transport current respectively. The specification of the Roebel strand and cable considered for this investigation is mentioned in Table 3, with only variation in Robel angle which is taken as 35°.

At low relative transport current, the FEA loss values deviate from the Norris formula (strip). However, the FEA results agrees well with the Norris formula (strip) at high relative transport current. Relative transport current is the ratio of the applied current to the critical current in the cable. In the magnetization case also the FEA loss data shows variation from the Brandt formula. The deviation occurs due to the inhomogeneous distribution of current density generated in the Roebel strand during the FE simulation of both transport current and magnetization case.

Fig. 17 reveals that the simulated results of Roebel cable deviate from the experimental data only at a very low magnetic field. No remarkable variation is noted between the results after 0.02T. Fig. 18 shows that the simulated results of Roebel cable are well matched to the experimental data when the applied current is from $0.4I_c$ to I_c. However, the FEA underestimates the experimental data from $0.1I_c$ to $0.3I_c$ (i.e. at low transport current values). The deviations are due to the fact that, the 3D model of FEA considered only the superconducting ReBCO layer for the AC loss simulation. However, while estimating the AC loss of a Roebel cable during experiment, all the layers in HTS tape are present. Hence, other losses such as eddy current loss in the stabilising layers and ferromagnetic loss in the substrates can also contribute to the total AC loss [21].

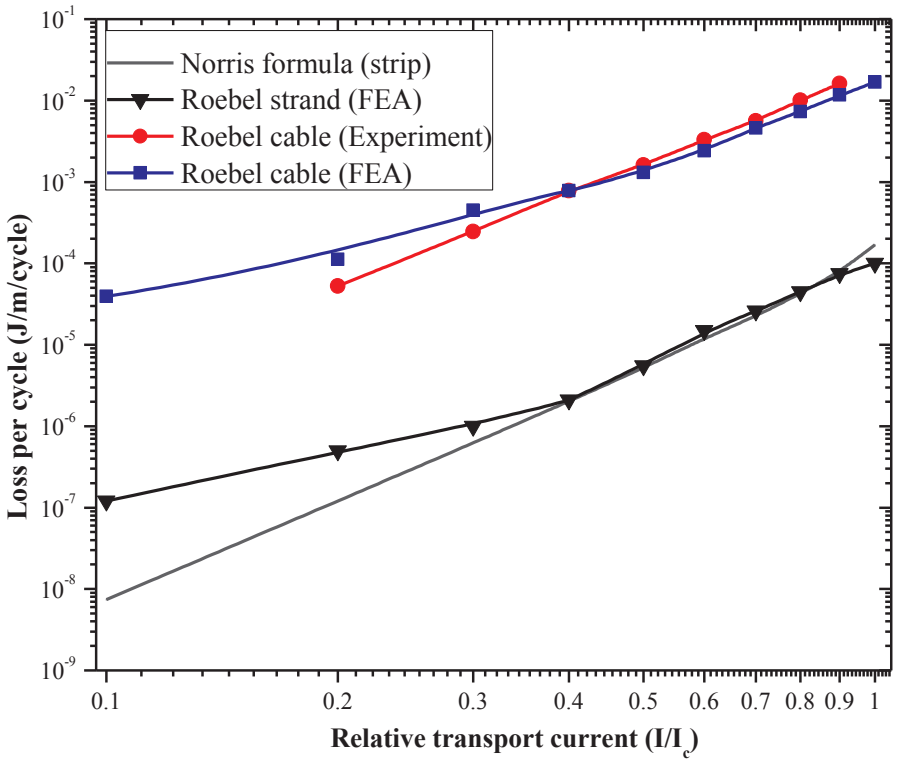

Fig. 18. AC losses in Roebel strand and cable for transport current case. FEA data were obtained from the simulation. Data points labelled Norris formula were calculated using the Norris formula for thin strip [24]. Experimental data were taken from [18].

3.4. Simulation method

First, a 14-strand Roebel cable with specification mentioned in Table 3 is modelled and its electromagnetic investigation is performed. The cable is then assumed as the default Roebel cable or default model. Two test cases were considered: i) Magnetization ii) Transport current. In the first case, the cable with no transport current is exposed to an alternating magnetic field (varying from 0.01T to 0.1T) perpendicular to its widest face. In the second case, an alternating current is applied to the cable (varying from $0.1I_c$ to I_c) which is free from any external magnetic field. Each geometrical parameters of the Roebel strand are then varied with respect to the default geometry and its AC loss under above two mentioned test cases were simulated. The obtained result is then compared with the default geometry and the influence of varying geometrical parameters on the electromagnetic behavior of the Roebel cable is studied.

The surface plot of the AC loss observed in the default geometry Roebel cable under the two test cases (magnetization and

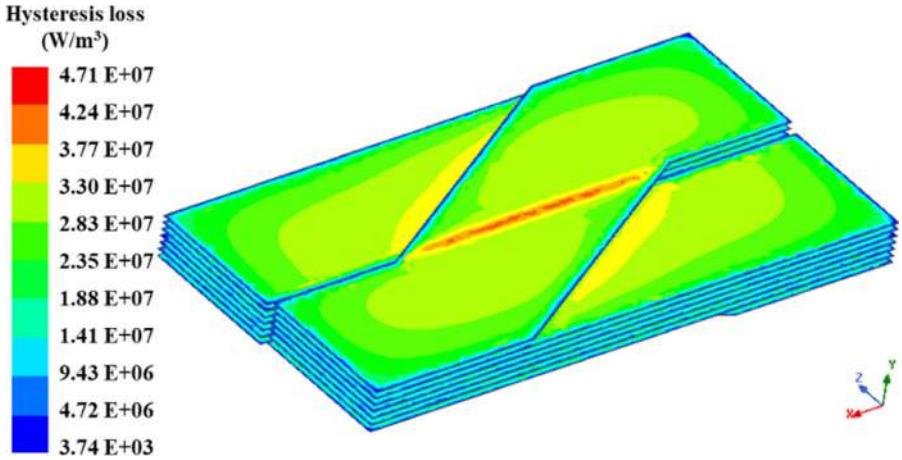

Fig. 19. Surface plot of the magnetization loss in the default geometry (Roebel cable).

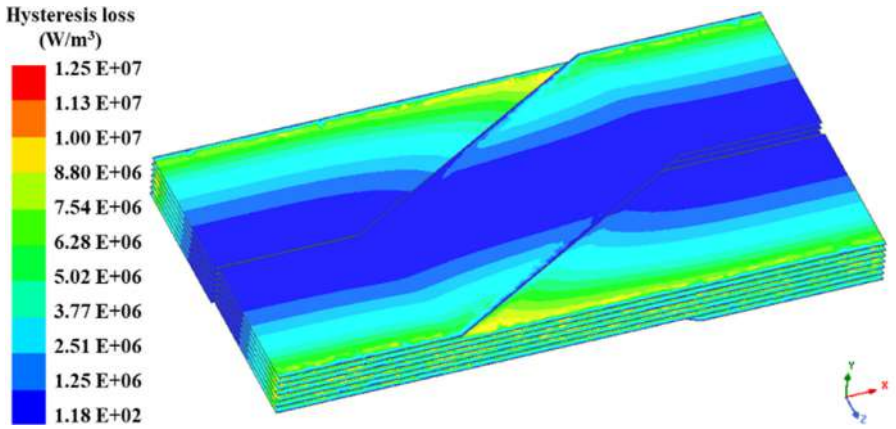

Fig. 20. Surface plot of the transport current loss in the default geometry (Roebel cable).

transport current cases) mentioned above are represented in Fig. 19 and Fig. 20 respectively. The dispersion of AC losses in a Roebel cable is comparable with that presented in [25]. In the present work, for the transport current case, it is considered that the supplied current is distributed in all the 14 strands equally. The average of the result obtained from the simulation of the respective model under consideration against an applied load condition is considered for further analysis and comparison.

For simplifying the analysis and better comparison with the default geometry, the relative values of AC loss and current density is taken. Relative value means the ratio of the estimated value from the simulation of the Roebel cable under consideration to the default geometrical configuration of the Roebel cable.

3.5. Result and discussions

Even though the model perceives all 14 strands of the Roebel cable, the surface plot and dispersion profile of current density is mapped only in the cross-over region of a specific strand to obtain a clarity in visualization. In all other regions of the strand (i.e at straight section), the current density is almost uniform and hence no variation in the distribution profile. All the geometries under consideration are exposed to a magnetic field varying from 0.01T to 0.1T. Similarly in the transport current case; the considered model are applied with an alternating current varying from $0.1I_c$ to I_c. The simulated result shows that the current density and AC loss distribution profile of all geometries differ only in their magnitude. Their relative values for a particular case considered also found equal. Hence, only three load cases were considered for plotting the graph which include 0.01T, 0.05T and 0.1T for the magnetization case and $0.1I_c$, $0.5I_c$ and I_c for the transport current case.

3.5.1. Magnetization losses

In superconducting cables, when a strand is subjected to an external magnetic field, it will oppose the effect by developing a magnetic field generated by the induced shielding (demagnetization) current of individual strands [11]. Hence, the AC loss of a Roebel cable with a particular geometrical configuration and number of strands depend on the intensity, distribution pattern and effect of shielding current developed against an applied magnetic field.

The comparison of loss due to magnetization obtained from the simulation of varying the size of outer fillet is represented in Fig. 21. It is noticed that providing fillet at the outer corner, increases the AC loss. However, the deviation is not apparent as the fillet dimension increases. Providing outer fillet in a Roebel strand causes a small reduction in material at the straight portion of the Roebel cable which affect the amount of screening current at this portion and result in slight increase in AC loss [11]. The increase in AC loss from outer corner sharp to a fillet dimension of 6 mm is only 0.51%.

Fig. 22 shows the difference in the current density distribution profile for the magnetization case of a Roebel strand at its cross-over region with variation in the outer fillet dimension. The surface plot of the current density at three different fillet dimensions are clearly indicated in the figure. The maximum magnetization current are noticed at the edges and at the cross-over region of the strand. From the figure, it is clear that providing outer fillet reduces the magnetization current density. However, the variation is not wide after 1 mm fillet.

The dependency of magnetization AC loss and current density with varying inner fillet dimension is represented in Fig. 23. Providing fillet at the inner corner increases the AC loss. However, it is to be noted that the percentage increase of loss from sharp inner corner to 6 mm fillet is only 0.69%. Providing inner fillet increase the proportion of area at the transposition region of the Roebel strand which is less affected by the screening (demagnetization) current of other strands resulting in a slight increase in AC loss [11]. Providing inner fillet causes a sharp decrease in current density, thereafter the variation seems feeble for all other fillet dimensions.

Fig. 24 shows the difference in the current density distribution profile for the magnetization case of a Roebel strand at its cross-over region with variation in the outer fillet dimension. Providing inner fillet increases the cross sectional area of the strand by a small amount and a corresponding fluctuation occurs in the developed screening current which is the main reason variation in

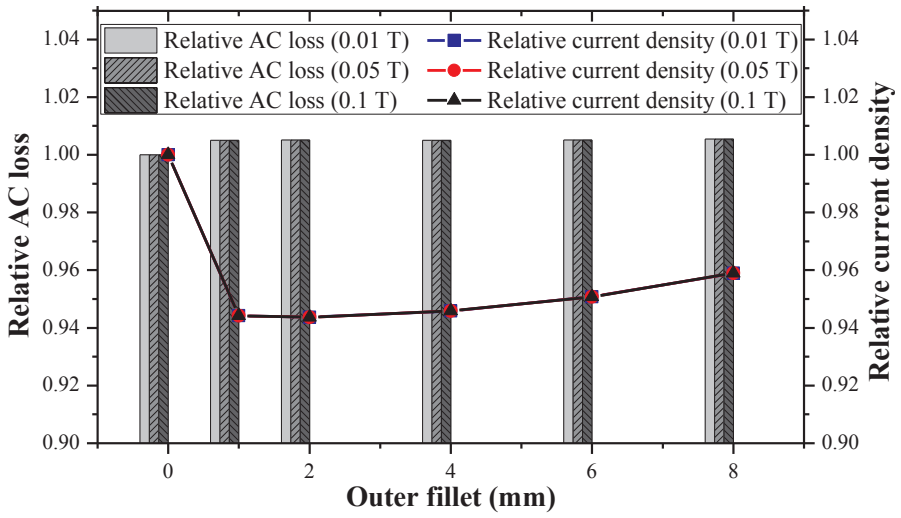

Fig. 21. Graph showing the variation of AC loss and current density with increase in outer fillet dimension.

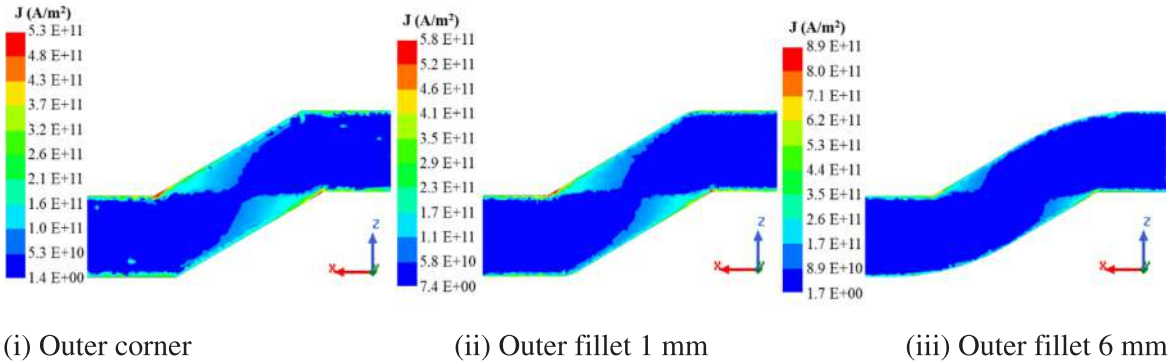

(i) Outer corner (ii) Outer fillet 1 mm (iii) Outer fillet 6 mm

Fig. 22. The current density distribution profile for the magnetization case (0.05T) of Roebel strand in its cross-over region for different sizes of outer fillet.

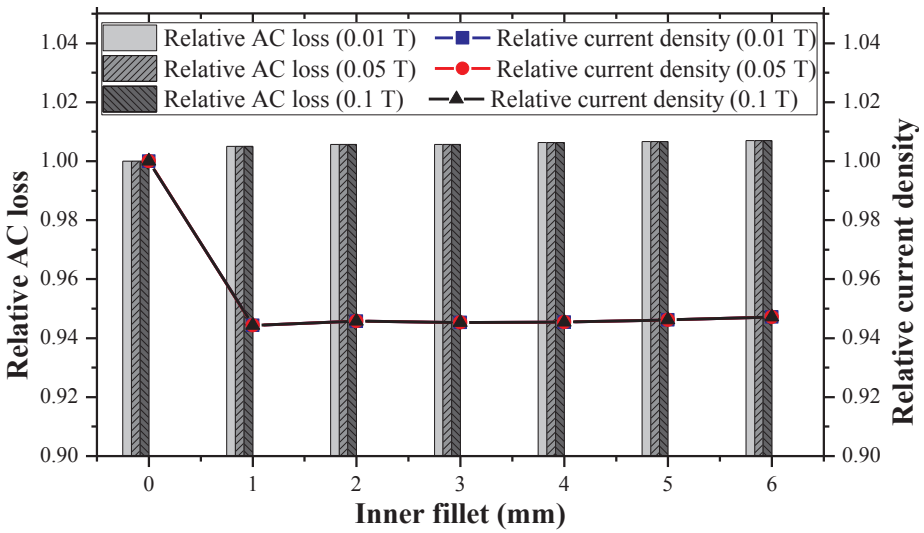

Fig. 23. Graph showing the variation of AC loss and current density with increase in inner fillet dimension.

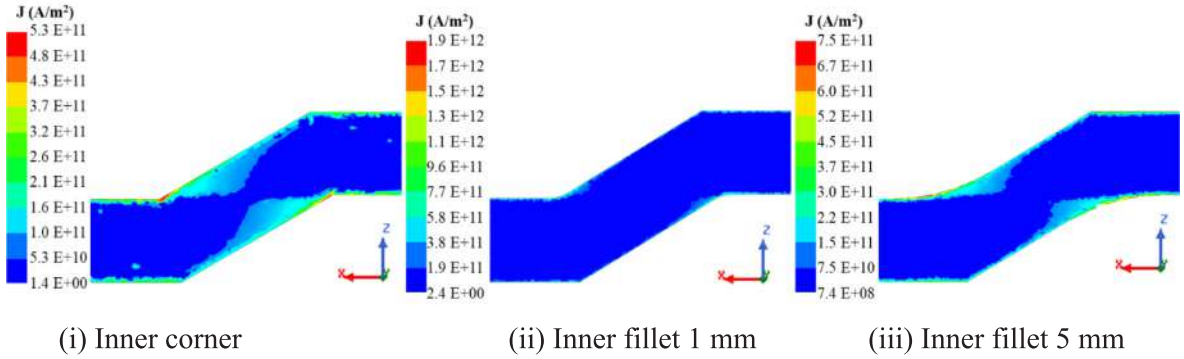

Fig. 24. The current density distribution profile for the magnetization case (0.05T) of Roebel strand in its cross-over region for different sizes of inner fillet.

current density.

The influence of varying Roebel angle in magnetization loss and current density of a Roebel cable can be inferred from the Fig. 25. As Roebel angle increases, the loss and current density reduces. The magnetization loss of a Roebel cable at straight section is less than that at the transposition section. As the effective area of straight section in a Roebel cable increases, the magnetization AC loss reduces. Since the number of strands passes over other strands at the cross-over region is less compared to the straight section, the demagnetization effect is also less which increase the magnetization loss at this portion of the Roebel cable [11]. From the careful observation of the geometrical structure of the 14-strand Roebel cable, it is noticed that as the Roebel angle increases, the effective area of the straight section increases which results the reduced AC loss of the cable.

The current density distribution profile of Roebel strands with different Roebel angles at the cross-over region is presented in Fig. 26. The maximum current density is noticed at the transposition region of the Roebel strand. When Roebel angle increases the current density decreases, because the transposition area and the maximum current density area of Roebel strand decreases with increase in Roebel angle.

The influence of varying strand's relative width on the AC loss and current density of a 14-strand Roebel cable is represented in Fig. 27. An increase in relative width of the strand causes only a small difference in the magnetization AC loss of the Roebel cable. There is no difference in the distribution profile of the AC loss when the relative width is varied from 1 to 2. It is stated in [26] that if the magnetic field is applied perpendicular to the cable, the hysteresis loss get reduced as the screening current developed in the strand prevents the flux penetration into the cable. When the relative width increases, the distribution and pattern of the screening

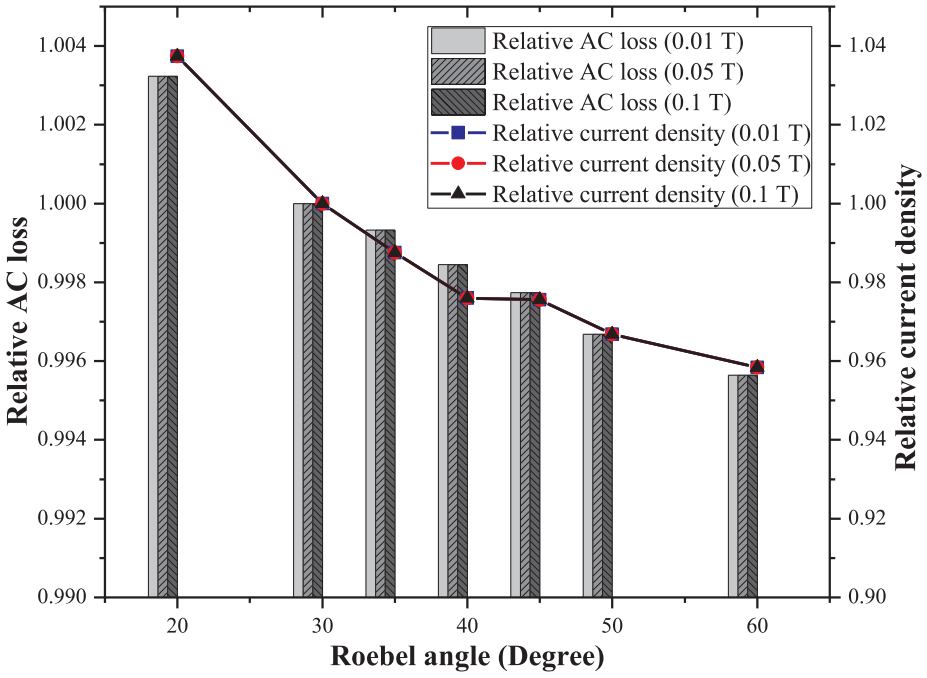

Fig. 25. Graph showing the variation of AC loss and current density with increase in Roebel angle.

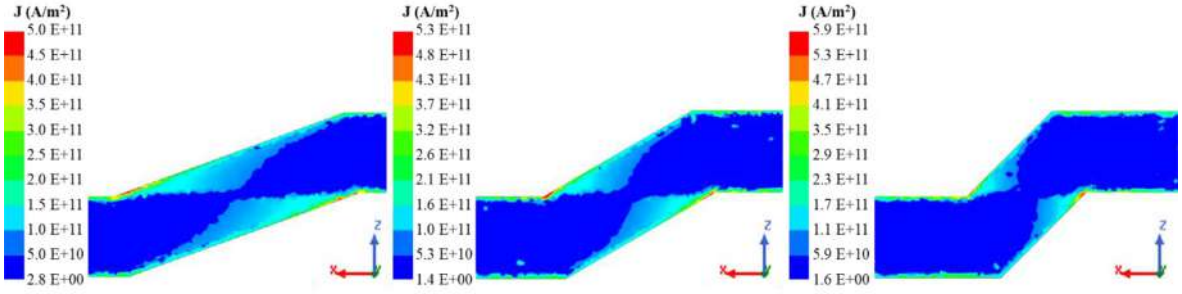

(i) Roebel angle = 20° (ii) Roebel angle = 30° (iii) Roebel angle = 45°

Fig. 26. The current density distribution profile for the magnetization case (0.05T) of Roebel strands with different Roebel angle at the cross-over region.

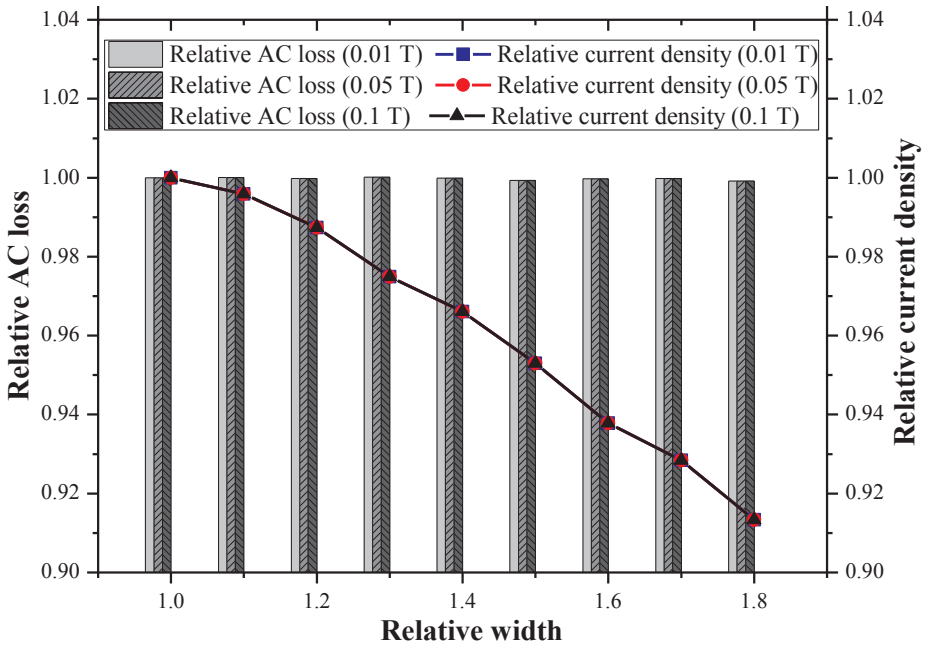

Fig. 27. Graph showing the variation of AC loss and current density with increase in relative width of the strand.

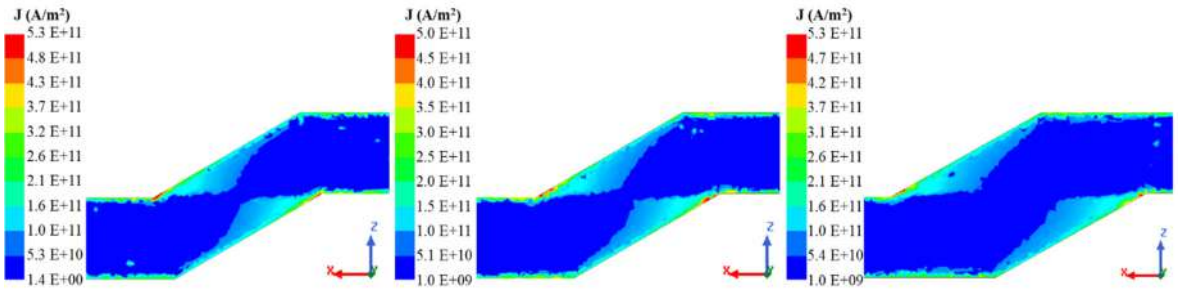

(i) Relative width = 1 (ii) Relative width = 1.1 (iii) Relative width = 1.5

Fig. 28. The current density distribution profile for the magnetization case (0.05T) of Roebel strands with different relative width. Colour scale indicates the intensity of current density.

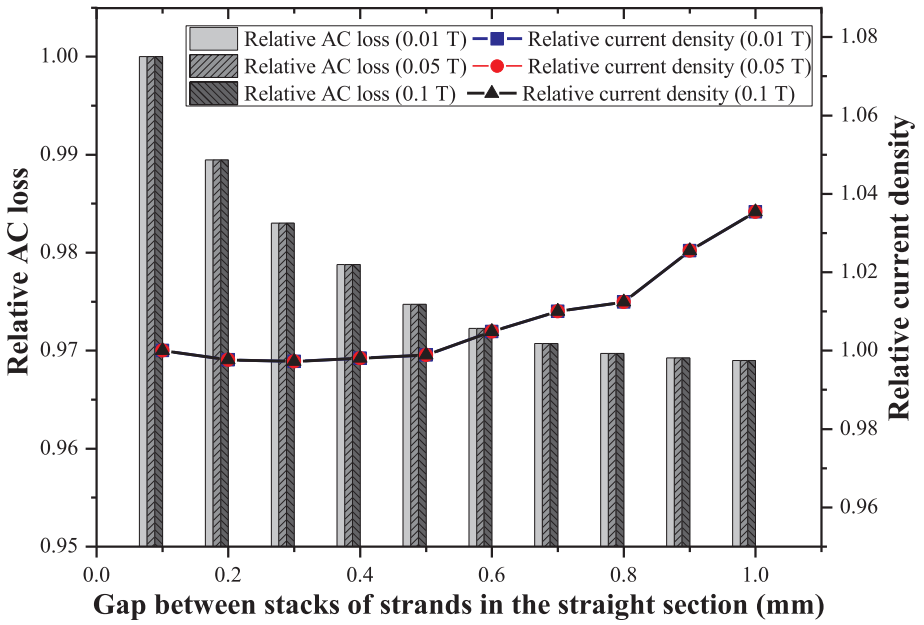

Fig. 29. Graph showing the variation of AC loss and current density with increase in gap between stacks of strands in the straight section of a Roebel cable.

current developed in the transposition region varies; this renders the penetration of more magnetic field lines and hence the total loss get varied.

The current density distribution profile of Roebel strands with different relative width is shown in Fig. 28. Increase in relative width increases the available cross sectional area of the conductor. Since the average current density obtained does not change significantly with increase in cross width of the strand, the current density decreases with increase in the relative width of the Roebel strand.

Fig. 29 represents the effect of changing gap between stacks of strand at the straight section of a Roebel cable on its AC loss and current density. Increasing the distance between the stacks of strands at the two straight rows of the Roebel cable cause a reduction in AC loss. First the variation is wide, however, as the distance increases the variation becomes narrow.

It is reported in [11] that the dependence of AC loss on the gap between stacks of strands at the straight section of the Roebel cable relies on the combined localized effect of loss in the straight and transposition region of the Roebel cable. At the straight portion of the Roebel cable, increasing the gap reduces AC loss and at the transposition region, increasing the gap increases AC loss. Hence, the loss also depends on the number and the transposition length of the strand, because the increase in strand number increases the proportion of the transposition area and increase in transposition length increase the proportion of straight region. In a 14-strand Roebel cable presented in this paper, it is observed that the AC loss decreases when the gap between stacks of strands at the straight section increases. The transposition area exposed to perpendicular magnetic field increases with increase in gap between stacks of strands in the straight section of the Roebel cable. Hence the screening current induced in the cable also increases. Since the cross sectional area of the strand remains constant, the current density increases with increase in gap between stacks of strands in the straight section of the Roebel cable.

3.5.2. Transport current losses

Transport current losses of Roebel cables without externally applied magnetic field are calculated by varying various geometrical configurations of the 3D model such as: inner and outer fillet dimensions, Roebel angle, relative width, gap between stacks of strands in the straight section of the Roebel cable. The surface plot of the current density obtained from the simulated result of various models presented in this session shows that, at the inner and outer corners of the Roebel strand, the current density is less than that of the other portions of the Roebel strand, which is consistent with the result mentioned in [27]. The change in geometrical parameters of the Roebel strand influences the smooth flow and even distribution of current through the conductor, which in turn adversely affect the cable performance and results in AC loss. It is also reported in [28] that the increase in superposition area of strand at straight section increase transport AC loss. The variation of available area at the straight section of a Roebel cable due to variation in strand parameter has already been explained in the magnetization session.

The effect of varying strand's outer fillet dimension on transport current AC loss and current density of a 14-strand Roebel cable is represented in Fig. 30. It can be noticed from the figure that the AC loss and current density increases as the size of outer fillet increases. An increase of 1.83% is observed when the fillet is varied from outer corner sharp to 6 mm. The obtained result is a clear indication that providing an outer fillet adversely affects the performance of the Roebel cable both during transport current and magnetization case.

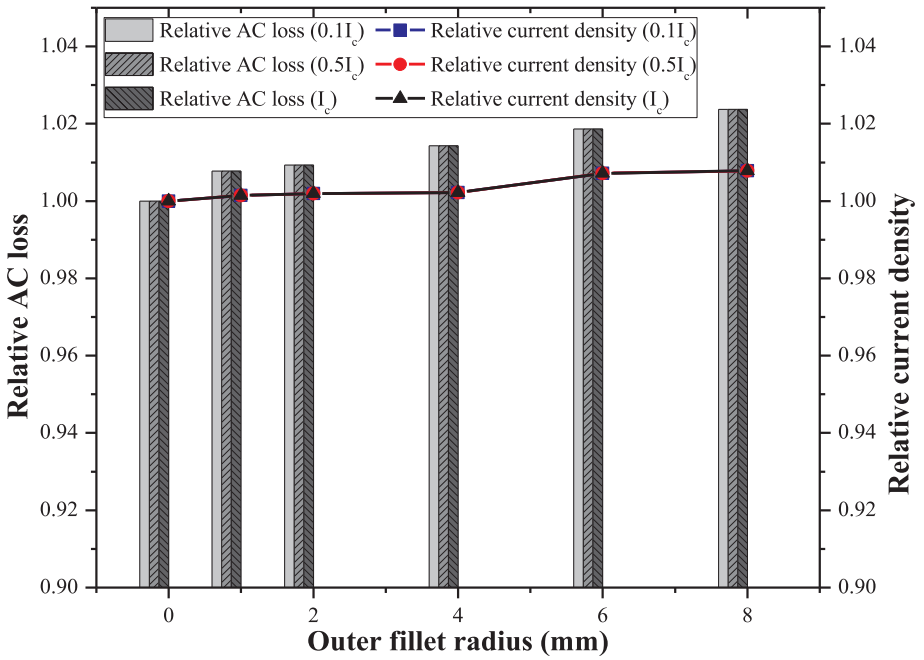

Fig. 30. Chart comparing the variation of AC loss and current density with increase in outer fillet dimension.

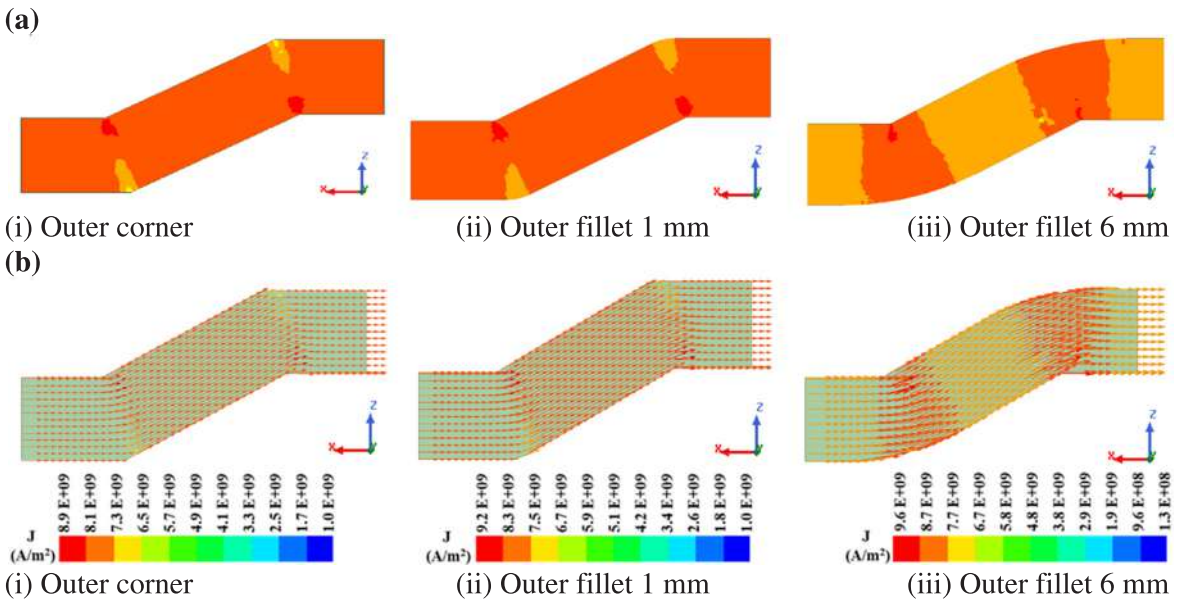

Fig. 31. The current density distribution profile for the transport current case (0.5I$_c$) of Roebel strand in its cross-over region for different sizes of outer fillet. (a) The surface plot of current density. (b) The vector distribution profile of current density.

Fig. 31 shows the difference in the current density distribution profile of a Roebel strand at its cross-over region with variation in the outer fillet dimension. The surface plot and the vector distribution profile of the current density at three different fillet dimensions are clearly indicated in the figure. The current density at all straight sections of the Roebel strand remains constant. However, the variation is severe in the cross-over region as the outer fillet dimension increases, which is not recommended for a good conductor. As the fillet dimension increases, the width of the strand at the beginning of the cross over region reduces due to material removal, since there is no variation in the magnitude of applied current, the density of current at the beginning of cross-over region increases. Hence, an unevenness in the distribution of current density occurs with increasing outer fillet radius.

The influence of providing inner fillet on the AC loss and current density of a 14-strand Roebel cable supplied with an alternating transport current is shown in Fig. 32. From the figure one can note that as the dimension of inner fillet increases, the loss also increases. However, the deviation is small compared to the AC loss occurred while varying the outer fillet. The percentage increase of

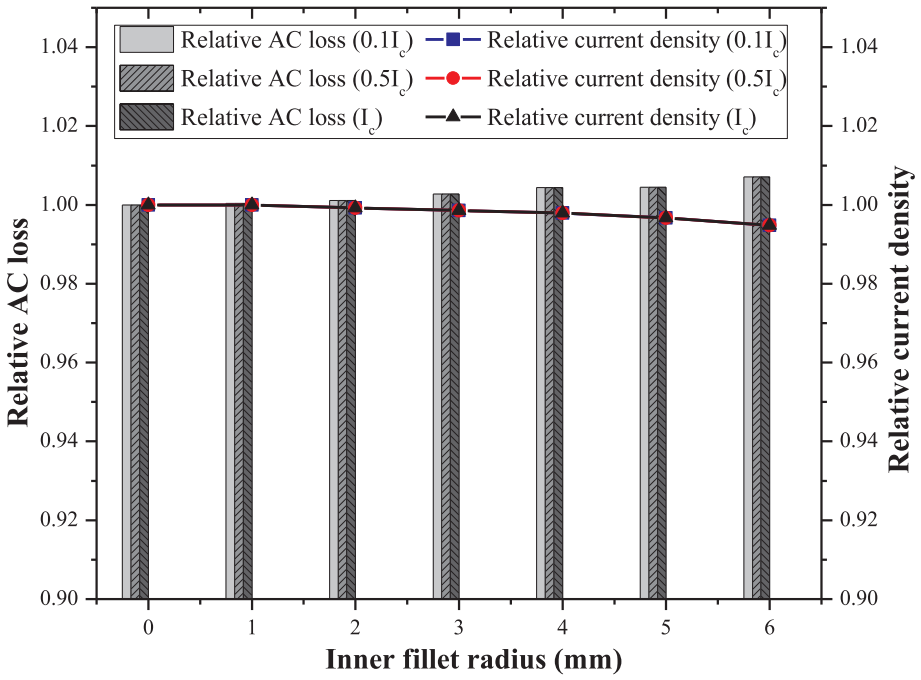

Fig. 32. Chart comparing the variation of AC loss and current density with increase in inner fillet dimension.

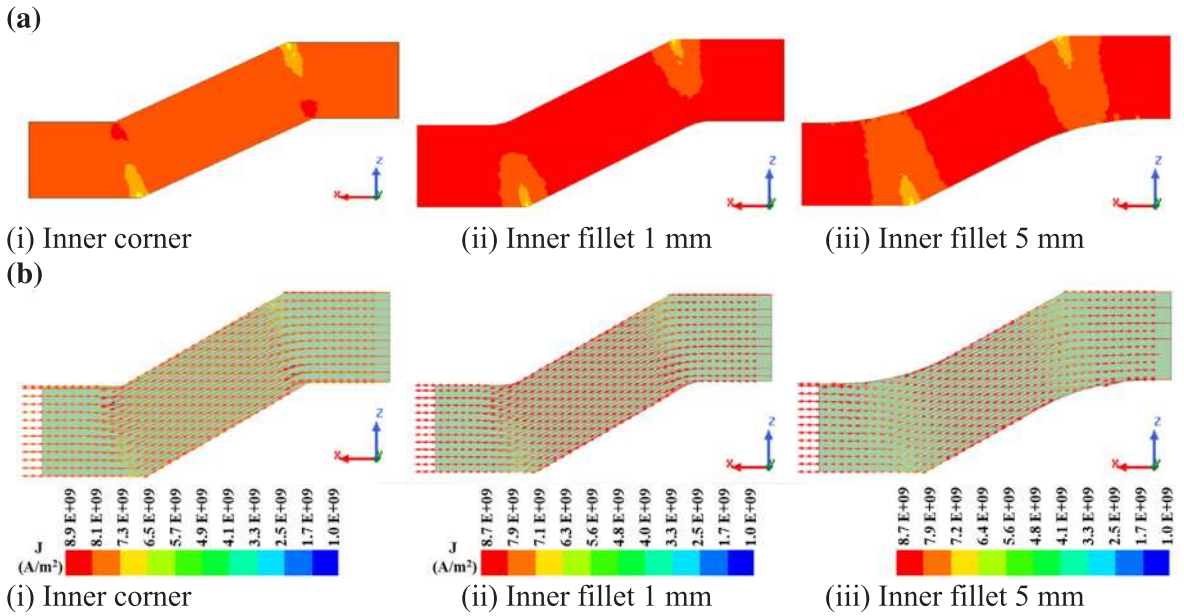

Fig. 33. The current density distribution profile for the transport current case (0.5I$_c$) of Roebel strand in its cross-over region for different sizes of inner fillet. (a) The surface plot of current density. (b) The vector distribution profile of current density.

loss from sharp inner corner to 6 mm fillet is only 0.71%.

The current density distribution profile of a Roebel strand in its cross-over region with variation in the inner fillet dimension is presented in Fig. 33. The surface plot and the vector distribution profile of the current density at three different fillet dimensions are also shown in the figure. From the figure, it can be inferred that providing inner fillet also induces some variation in the distribution of current density in a Roebel strand. However, the variation not severe compared to that of providing outer fillet. Also, it is observed that the current density is affected only at the beginning of the cross-over region; at all the other regions, the current density is evenly distributed. In contradiction to that of the outer fillet case, providing an inner fillet and increasing its dimension reduces the current density. However, similar to that of the outer fillet case, the unevenness of current density at the transposition section of the Roebel

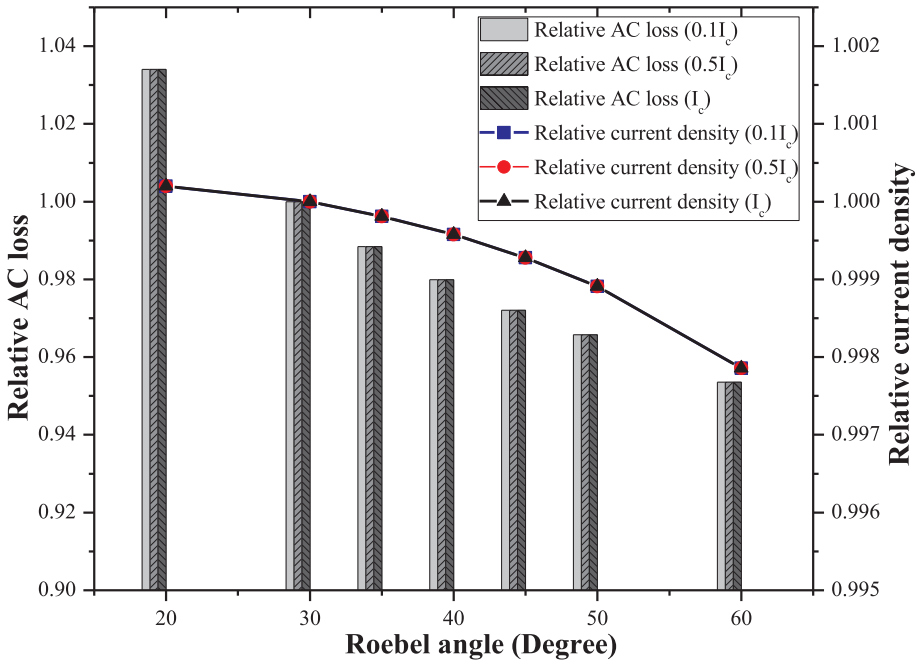

Fig. 34. Chart comparing the variation of AC loss and current density with increase in Roebel angle.

cable increases with increase in inner fillet dimension, which is the main reason for the increase in AC loss.

A graphical representation of the effect of increasing Roebel angle on the transport current loss and current density of a 14-strand Roebel cable is given in Fig. 34. The figure shows that the AC loss and the current density reduces as Roebel angle increases.

The current density distribution profile of Roebel strands with different Roebel angle at the cross-over region is presented in Fig. 35. The surface plot and the vector distribution profile of the current density at three different Roebel angles are shown. The figure shows that the corners become sharper as the Roebel angle increases and it adversely affects the distribution of current in the strand. Also in some regions of the cross-over region, especially at the corners, the current density varies a lot and this phenomenon increase as the Roebel angle increases. This reduces the proportion of uniform current density area. Hence, even though the AC loss decreases marginally with an increase in Roebel angle, it is not advisable to increase the Roebel angle beyond a certain limit as it

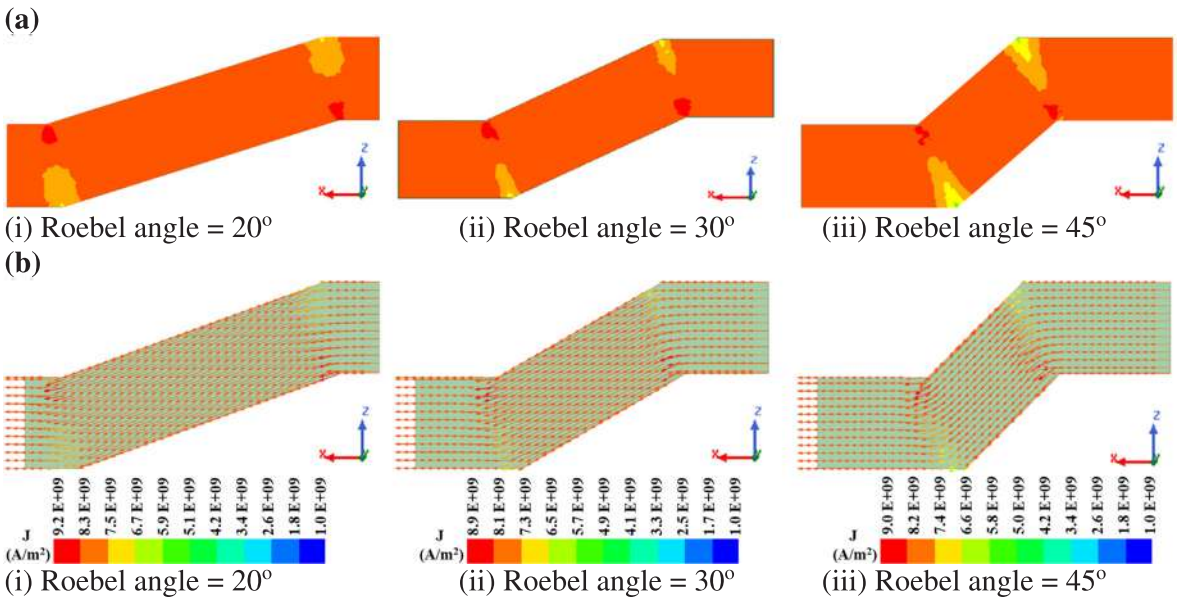

Fig. 35. The current density distribution profile for the transport current case (0.5I$_c$) of Roebel strands with different Roebel angle at the cross-over region. (a) The surface plot of current density. (b) The vector distribution profile of current density.

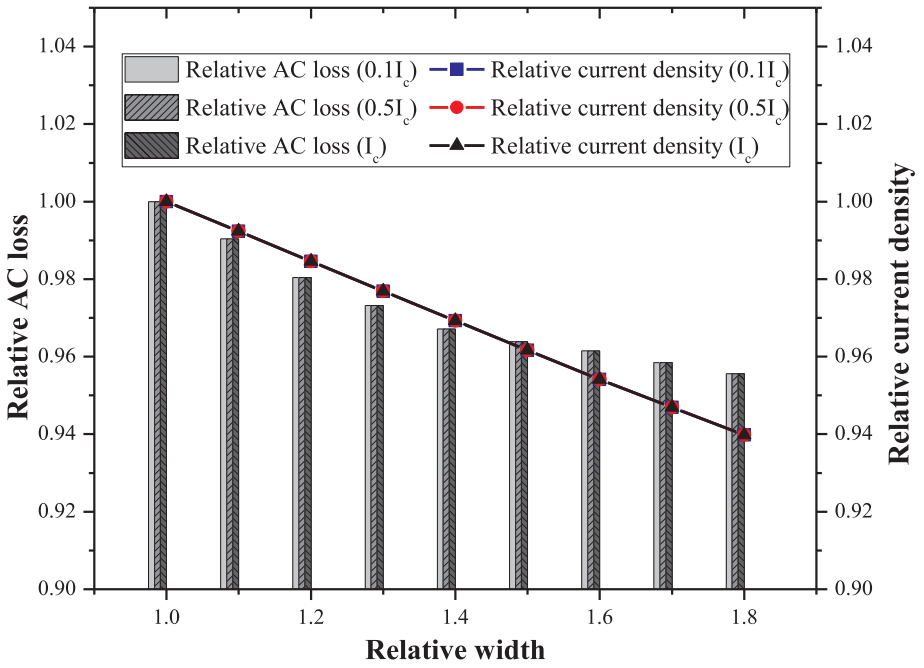

Fig. 36. Chart comparing the variation of AC loss and current density with increase in relative width of Roebel strand.

adversely affects the uniform distribution of current through the strand. The authors [8] suggests a Roebel angle of 35° for a Robel strand with inner fillet 6 mm, outer corner sharp, relative width 1.2 and transposition length of 180 mm.

The dependency of relative width on AC loss and current density of a 14-strand Roebel cable is indicated in Fig. 36. Figure shows that the AC loss and current density reduces as relative width increases.

The current density distribution profile of Roebel strands with different relative width is shown in Fig. 37. The surface plot and the vector distribution profile of the current density at three different relative widths are also shown. From the figure, it can be inferred that the increase in relative width of the cross over region reduces the current density at this portion since there is no variation in the magnitude of current flowing through the conductor. Hence the average current density of the whole conductor reduces which is clearly reflected in the graph shown in Fig. 36.

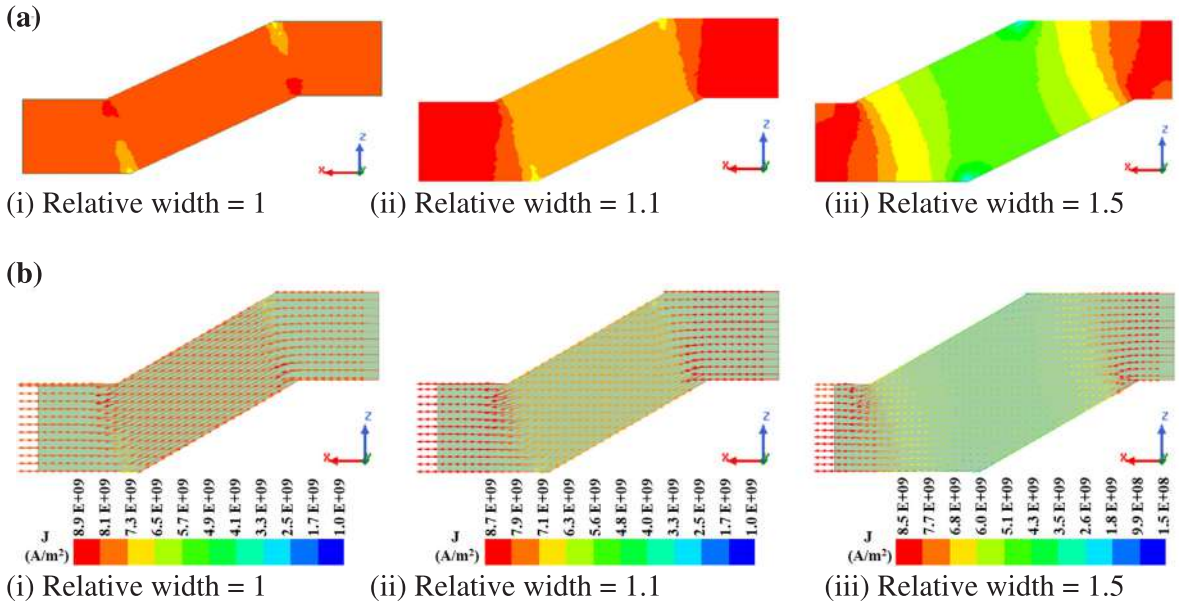

Fig. 37. The current density distribution profile for the transport current case (0.5I$_c$) of Roebel strands with different relative width. (a) The surface plot of current density. (b) The vector distribution profile of current density.

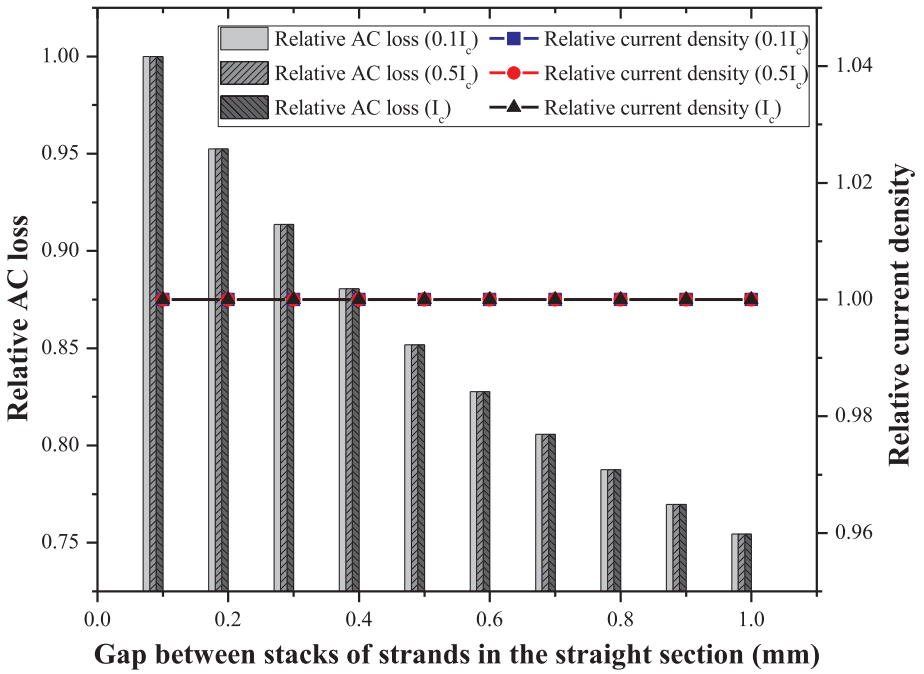

Fig. 38. Chart comparing the variation of AC loss and current density with increase in gap between stacks of strands in the straight section of the Roebel cable.

The influence of varying gap between stacks of strands in the straight section of the Roebel cable on the AC loss and current density of a 14-strand Roebel cable is depicted in Fig. 38. Figure shows that as the gap between stacks of strands at the straight section of the Roebel cable increases, the AC loss reduces. The increase in gap doesn't make any wide variation in the available solid cross sectional area of the Roebel cable for conducting current, hence the variation in current density is also negligible.

In the work done by [29], a successful comparison between the experimental and numerical analysis was performed in order to analyse the influence of increasing gap between stacks of strands of a Roebel cable in its transport AC loss characteristics and it is reported that the loss decreases as the gap increases. However, wide variation was not performed by the authors in the Roebel cable geometry and they used the Norris strip model which overlooked the transposition part of the Roebel strand. Analyzing the Fig. 38, we can infer that the present result is consistent with the result mentioned in [29].

The above results clarify that similar to that mentioned in [25], the 3D structure of Roebel cables and any variation in its parameters influence their response to AC loss.

4. Conclusion

In the present work, the influence of geometrical parameters on the electro-mechanical stability of Roebel cables is carefully investigated. The parameters such as inner fillet radius, outer fillet radius, Roebel angle, strand width at crossing section and the gap between stacks of strand in the straight section are varied and its influence on mechanical stability and electromagnetic characteristics are observed.

From the electro-mechanical analysis, it is observed that providing outer fillet will adversely affect the performance of the Roebel cable. Hence, the Roebel strand should always be punched off with its outer corner sharp from the HTS-tape.

Providing an inner fillet avoids the stress concentration developed due to external tensile load and distributes it over a wider area. Even though there will be slight increase in AC loss due to inner fillet, this variation is comparatively small. Hence it is recommended to provide suitable inner fillet while cutting Roebel strands of required dimension from the HTS tape as the mechanical stability of cable increases.

Increasing Roebel angle increases the mechanical stability of Roebel cable and also reduces the magnetization and transport current losses. However, the smooth flow of current through the conductor, especially at the transposition region, will be adversely get affected by the increase in Roebel angle. Hence, it is not advisable to increase the Roebel angle beyond the recommended limit.

An increase in relative width of the strand causes only a small difference in the magnetization AC loss of the Roebel cable, and the current density at the cross-over region get reduced. When the relative width of a Roebel strand increases, the applied load get distributed over a wider area in the cross-over region. However, too much increase is not experienced in the stability of the strand against applied tensile load. Since the increase in relative width greatly influence the space requirement of each strand in the Roebel cable, a relative width between 1 and 1.2 is recommended.

The dependence of AC loss on the gap between stacks of strands at the straight section of the Roebel cable relies on the combined

localized effect of loss in the straight and transposition region of the Roebel cable. At the straight portion of the Roebel cable, increasing the gap reduces AC loss and at the transposition region, increasing the gap increases AC loss. The increase in gap doesn't make any wide variation in the available solid cross sectional area of the Roebel cable for conducting current, hence the variation in current density is also negligible. As the gap between stacks of strand increases, due to the specific meander structure of the Roebel strand, most of the applied tensile load causes an uneven twist instead of being distributed into the strand. Hence the resulting axial strain in the ReBCO layer reduces and the strand fails at a lower strain even though applied strain on the Roebel strand is high.

The optimized geometry of a Roebel cable depends not only on its electro-magnetic behaviour but also on its performance against external applied loads. Selecting the right geometric configuration is very important to get a stable Roebel cable exhibiting long life.

Declaration of Competing Interest

The authors declare that they have no known competing financial interests or personal relationships that could have appeared to influence the work reported in this paper.

Acknowledgements

We acknowledge the Space Technology Laboratory under the Department of Mechanical Engineering, TKM College of Engineering, Karikode, Kollam, Kerala, India for providing the computational facilities.

Appendix A. Supplementary data

Supplementary data to this article can be found online at https://doi.org/10.1016/j.engfailanal.2020.104804.

References

[1] M.N. Wilson, Superconductivity and accelerators: The good companions, IEEE Trans. Appl. Supercond. 9 (1999) 111–121, https://doi.org/10.1109/77.783250.
[2] W. Goldacker, R. Nast, G. Kotzyba, S.I. Schlachter, A. Frank, B. Ringsdorf, C. Schmidt, P. Komarek, High current DyBCO-ROEBEL Assembled Coated Conductor (RACC), J. Phys. Conf. Ser. 43 (2006) 901–904, https://doi.org/10.1088/1742-6596/43/1/220.
[3] D.C. Van Der Laan, YBa2Cu3O7-δ coated conductor cabling for low ac-loss and high-field magnet applications, Supercond. Sci. Technol. 22 (2009) 065013, , https://doi.org/10.1088/0953-2048/22/6/065013.
[4] M. Takayasu, F.J. Mangiarotti, L. Chiesa, L. Bromberg, J.V. Minervini, Conductor characterization of YBCO twisted stacked-tape cables, IEEE Trans. Appl. Supercond. 23 (2013) 4800104, https://doi.org/10.1109/TASC.2012.2234182.
[5] K.P. Thakur, Z. Jiang, M.P. Staines, N.J. Long, R.A. Badcock, A. Raj, Current carrying capability of HTS Roebel cable, Phys. C Supercond. Its Appl. 471 (2011) 42–47, https://doi.org/10.1016/j.physc.2010.11.001.
[6] A. Frank, R. Heller, W. Goldacker, A. Kling, C. Schmidt, Roebel assembled coated conductor cables (RACC): Ac-Losses and current carrying potential, J. Phys. Conf. Ser. 97 (2008) 012147, , https://doi.org/10.1088/1742-6596/97/1/012147.
[7] C.W. Bumby, R.A. Badcock, N.J. Long, Critical current behavior of HTS Roebel cable under tensile stress, IEEE Trans. Appl. Supercond. 23 (2013) 4801805, https://doi.org/10.1109/TASC.2013.2243897.
[8] C. Barth, K.P. Weiss, M. Vojenčiak, S. Schlachter, Electro-mechanical analysis of Roebel cables with different geometries, Supercond. Sci. Technol. 25 (2011) 025007, , https://doi.org/10.1088/0953-2048/25/2/025007.
[9] M. Vojenčiak, F. Grilli, S. Terzieva, W. Goldacker, M. Kováčová, A. Kling, Effect of self-field on the current distribution in Roebel-assembled coated conductor cables, Supercond. Sci. Technol. 24 (2011) 095002, , https://doi.org/10.1088/0953-2048/24/9/095002.
[10] Z. Jiang, M. Staines, N.J. Long, R.A. Badcock, C. Bumby, E. Talantsev, K. Hamilton, R.G. Buckley, N. Amemiya, The scaling of transport AC losses in Roebel cables with varying strand parameters, Supercond. Sci. Technol. 27 (2014) 075007, , https://doi.org/10.1088/0953-2048/27/7/075007.
[11] T. Tsukamoto, T. Mifune, Y. Sogabe, Z. Jiang, T. Nakamura, N. Amemiya, Influence of geometrical configurations of HTS Roebel cables on their AC losses, IEEE Trans. Appl. Supercond. 25 (2015) 4802005, https://doi.org/10.1109/TASC.2014.2368056.
[12] D.W. Hazelton, Progress in Coated Conductor at SuperPower, http://www.Superpower-Inc.Com/Content/Technical-Documents. (2010).
[13] K. Osamura, M. Sugano, S. MacHiya, H. Adachi, S. Ochiai, M. Sato, Internal residual strain and critical current maximum of a surrounded Cu stabilized YBCO coated conductor, Supercond. Sci. Technol. 22 (2009) 065001, , https://doi.org/10.1088/0953-2048/22/6/065001.
[14] K. Ilin, K.A. Yagotintsev, C. Zhou, P. Gao, J. Kosse, S.J. Otten, W.A.J. Wessel, T.J. Haugan, D.C. Van Der Laan, A. Nijhuis, Experiments and FE modeling of stress-strain state in ReBCO tape under tensile, torsional and transverse load, Supercond. Sci. Technol. 28 (2015) 055006, , https://doi.org/10.1088/0953-2048/28/5/055006.
[15] N.J. Long, R. Badcock, P. Beck, M. Mulholl, N. Ross, M. Staines, H. Sun, J. Hamilton, R.G. Buckley, Narrow strand YBCO Roebel cable for lowered AC loss, J. Phys. Conf. Ser. 97 (2008) 012280, , https://doi.org/10.1088/1742-6596/97/1/012280.
[16] W. Goldacker, A. Frank, A. Kudymow, R. Heller, A. Kling, S. Terzieva, C. Schmidt, Status of high transport current ROEBEL assembled coated conductor cables, Supercond. Sci. Technol. 22 (2009) 034003, , https://doi.org/10.1088/0953-2048/22/3/034003.
[17] W. Goldacker, A. Frank, R. Heller, S.I. Schlachter, B. Ringsdorf, K.P. Weiss, C. Schmidt, S. Schuller, ROEBEL Assembled Coated Conductors (RACC): Preparation, properties and progress, IEEE Trans. Appl. Supercond. 17 (2007) 3398–3401, https://doi.org/10.1109/TASC.2007.899417.
[18] V.M.R. Zermeno, F. Grilli, F. Sirois, A full 3D time-dependent electromagnetic model for Roebel cables, Supercond. Sci. Technol. 26 (2013) 052001, , https://doi.org/10.1088/0953-2048/26/5/052001.
[19] S. Gijoy, K.E.R. Roy, 3D Finite Element Electromagnetic Analysis of a 14-Strand HTS Roebel Cable, J. Supercond. Nov. Magn. 33 (2020) 1709–1719, https://doi.org/10.1007/s10948-020-05465-7.
[20] S. Terzieva, M. Vojenčiak, E. Pardo, F. Grilli, A. Drechsler, A. Kling, A. Kudymow, F. Gömöry, W. Goldacker, Transport and magnetization ac losses of ROEBEL assembled coated conductor cables: measurements and calculations, Supercond. Sci. Technol. 23 (2010) 014023, , https://doi.org/10.1088/0953-2048/23/1/014023.
[21] F. Grilli, E. Pardo, A. Stenvall, D.N. Nguyen, W. Yuan, F. Gomory, Computation of losses in HTS under the action of varying magnetic fields and currents, IEEE Trans. Appl. Supercond. 24 (2013) 78–110, https://doi.org/10.1109/TASC.2013.2259827.
[22] J. Van Nugteren, B. Van Nugteren, P. Gao, L. Bottura, M. Dhallé, W. Goldacker, A. Kario, H. Ten Kate, G. Kirby, E. Krooshoop, G. De Rijk, L. Rossi, C. Senatore, S. Wessel, K. Yagotintsev, Y. Yang, Measurement and Numerical Evaluation of AC Losses in a ReBCO Roebel Cable at 4.5 K, IEEE Trans. Appl. Supercond. 26 (2016) 8201407, https://doi.org/10.1109/TASC.2016.2525919.
[23] E.H. Brandt, M. Indenbom, Type-II-superconductor strip with current in a perpendicular magnetic field, Phys. Rev. B. 48 (1993) 12893–12906, https://doi.org/

10.1209/0295-5075/22/9/017.
[24] W.T. Norris, Calculation of hysteresis losses in hard superconductors carrying ac: isolated conductors and edges of thin sheets, J. Phys. D. Appl. Phys. 3 (1970) 489–507, https://doi.org/10.1088/0022-3727/3/4/308.
[25] N. Amemiya, T. Tsukamoto, M. Nii, T. Komeda, T. Nakamura, Z. Jiang, Alternating current loss characteristics of a Roebel cable consisting of coated conductors and a three-dimensional structure, Supercond. Sci. Technol. 27 (2014) 035007, , https://doi.org/10.1088/0953-2048/27/3/035007.
[26] L.S. Lakshmi, M.P. Staines, K.P. Thakur, R.A. Badcock, N.J. Long, Frequency dependence of magnetic ac loss in a five strand YBCO Roebel cable, Supercond. Sci. Technol. 23 (2010) 065008, , https://doi.org/10.1088/0953-2048/23/6/065008.
[27] J. Emhofer, F. Hengstberger, M. Eisterer, H.W. Weber, S. Terzieva, W. Goldacker, R.A. Badcock, N.J. Long, Current and field distribution in meandered coated conductors for roebel cables, IEEE Trans. Appl. Supercond. 21 (2011) 3389–3392, https://doi.org/10.1109/TASC.2010.2092394.
[28] Z. Jiang, R.A. Badcock, N.J. Long, M. Staines, K.P. Thakur, L.S. Lakshmi, A. Wright, K. Hamilton, G.N. Sidorov, R.G. Buckley, N. Amemiya, A.D. Caplin, Transport AC loss characteristics of a nine strand YBCO Roebel cable, Supercond. Sci. Technol. 23 (2010) 025028, , https://doi.org/10.1088/0953-2048/23/2/025028.
[29] Z. Jiang, K.P. Thakur, N.J. Long, R.A. Badcock, M. Staines, Comparison of transport AC losses in an eight-strand YBCO Roebel cable and a four-tape YBCO stack, Phys. C Supercond. Its Appl. 471 (2011) 999–1002, https://doi.org/10.1016/j.physc.2011.05.109.